Defence Research and Development Canada
Recherche et développement pour la défense Canada

DEFENCE R&D DÉFENSE

Validation of ship signatures in Envisat ASAR AP mode data using AISLive

Data acquisition, processing, and analysis results

Paris W. Vachon and John Wolfe

Defence R&D Canada – Ottawa
TECHNICAL MEMORANDUM
DRDC Ottawa TM 2008-005
March 2008

Canada

Validation of ship signatures in Envisat ASAR AP mode data using AISLive

Data acquisition, processing, and analysis results

Paris W. Vachon
John Wolfe

DRDC Ottawa

Defence R&D Canada – Ottawa

Technical Memorandum
DRDC Ottawa TM 2008-005
March 2008

Principal Author

Original signed by Paris W. Vachon

Paris W. Vachon

Defence Scientist

Approved by

Original signed by Gary W. Geling

Gary W. Geling

Head, Radar Applications and Space Technologies

Approved for release by

Original signed by Pierre Lavoie

Pierre Lavoie

Chair, Document Review Panel

This work was supported in part by a Service Level Agreement between the Polar Epsilon Project Management Office and DRDC Ottawa.

Abstract

Ships appear in synthetic aperture radar (SAR) ocean imagery as bright targets against the ocean clutter background. Envisat Advanced SAR (ASAR) Alternating Polarization (AP) mode data acquisitions over the Strait of Dover and the Strait of Gibraltar, two high-density shipping regions with Automatic Identification System (AIS) coverage via AISLive, have provided a large database of validated ship signatures. For each validated ship signature, several metrics were computed including the clutter statistics, the total radar cross section of each ship, and the ship signature length. These metrics were evaluated in terms of the polarization, the local incidence angle, the validated ship length, the target to clutter ratio, and the ship aspect angle. This is a very rich data set that has yielded new observations and insights to ship detectability by SAR. These results could have bearing on the design of future SAR modes or SAR missions, and could be used to improve the performance of ship detection software.

Résumé

Sur les images de l'océan acquises au radar à synthèse d'ouverture (RSO), les navires apparaissent comme des cibles brillantes sur l'arrière-plan de fouillis d'échos. Des données acquises au moyen du RSO évolué (ASAR) de l'Envisat en mode de polarisation alternée (PA) sur le Pas de Calais et le détroit de Gibraltar, deux régions à grande densité d'activité maritime couvertes par le Système d'identification automatique (SIA en direct, par l'AISLive), ont fourni une grosse base de données de signatures de navires validées. Pour chaque signature de navire validée, plusieurs mesures ont été calculées dont les statistiques sur le fouillis d'échos, la section efficace en radar de chaque navire et la longueur de la signature du navire. Ces mesures ont été évaluées en termes de polarisation, d'angle d'incidence local, de longueur validée du navire, du rapport cible sur fouillis et d'angle d'aspect du navire. Il s'agit d'un très riche jeu de données qui a fourni de nouvelles observations et perspectives sur la détectabilité des navires au moyen du RSO. Ces résultats pourraient être importants pour la conception de futurs modes ou missions RSO et pourraient être utilisés pour l'amélioration du rendement des logiciels de détection de navires.

This page intentionally left blank.

Executive summary

Validation of ship signatures in Envisat ASAR AP mode data using AISLive: Data acquisition, processing, and analysis results

Vachon, Paris W.; Wolfe, John; DRDC Ottawa TM 2008-005; Defence R&D Canada – Ottawa; March 2008.

Introduction: Ships appear in synthetic aperture radar (SAR) ocean imagery as bright targets against the ocean clutter background. Envisat Advanced SAR (ASAR) Alternating Polarization (AP) mode data acquisitions over the Strait of Dover and the Strait of Gibraltar, two high-density shipping regions with Automatic Identification System (AIS) coverage via AISLive, a commercial AIS provider, have provided a large database of validated ship signatures that can be used to address the polarization dependence of ship detectability. The AIS data were in turn validated through the Internet Ships Register (ISR).

The analysis methods are similar to those used to analyze previously acquired RADARSAT-1 Fine and ScanSAR Narrow B mode data sets of ships validated by AISLive data.

Results: For each validated ship, several metrics were computed using the VUSAR image analysis tool. These included the clutter statistics, the total radar cross section (RCS) of each ship, and the ship signature length. These metrics were evaluated in terms the polarization, the local incidence angle, the validated ship length, the target to clutter ratio, and the ship aspect angle. The following is apparent:

- The cross-polarization ocean clutter is at the Envisat ASAR noise floor, so any target contrast metrics would be relative to the instrument noise floor rather than the ocean clutter;
- The background ocean clutter may be characterized as K-distributed;
- For the ship targets, the HH and VV total RCS are comparable while the cross-polarization total RCS is about 10 dB smaller than the co-polarization total RCS; models for the total RCS as a function of ship length are provided;
- For co-polarization, the ship target contrast increases with increasing incidence angle, while for cross-polarization the contrast is more-or-less independent of incidence angle; the co-polarization ship contrast is larger for cross-polarization if the incidence angle is smaller than 33°;
- The total RCS variability was successfully modelled by fitting the normalized total RCS to several well known probability density functions; the RCS variability is smaller for cross-polarization ship signatures;
- The ship signature length agreed with the validated ship length for 60.1% of the co-polarization ships and 71.5% of the cross-polarization ships; for co-polarization, the rate of underestimation of ship length is higher; for cross-polarization, the rate of overestimation of ship length is higher; there tends to be more overestimates of ship length for azimuth travelling ships;

- Ship wake signatures appear in the cross-polarization channel as a ship-like signature that has not been subject to azimuth shifting, as occurs for the ship signature itself; these signatures appear frequently and may be due to scattering from waves generated off the bow of the ship.

Significance: This is a very rich data set that has yielded new observations and insights to ship detectability by SAR. These results could have bearing on the design of future SAR modes or SAR missions, and could be used to improve the performance of ship detection software.

The use of AIS data for ship signature validation is now a well-proven methodology that should be used to develop ship detection models for other missions such as TerraSAR-X and Cosmos-Skymed. Focussing on high density shipping regions would provide a significant set of validated ship targets for each image acquired.

Sommaire

Validation of ship signatures in Envisat ASAR AP mode data using AISLive: Data acquisition, processing, and analysis results

Vachon, Paris W.; Wolfe, John; DRDC Ottawa TM 2008-005; R & D pour la défense Canada – Ottawa; Mars 2008.

Introduction ou contexte: Sur les images de l'océan acquises au radar à synthèse d'ouverture (RSO), les navires apparaissent comme des cibles brillantes sur l'arrière-plan de fouillis d'échos. Des données acquises au moyen du RSO évolué (ASAR) de l'Envisat en mode de polarisation alternée (PA) sur le Pas de Calais et le détroit de Gibraltar, deux régions à grande densité d'activité maritime couvertes par le Système d'identification automatique, SIA en direct, par l'AISLive, un fournisseur commercial du SIA, ont fourni une grosse base de données de signatures de navires validées qui peut être appliquée à la détermination de la dépendance de la détectabilité des navires à l'endroit de la polarisation. Les données du SIA ont été à leur tour validées d'après l'*Internet Ships Register* (ISR).

Les méthodes d'analyse sont similaires à celles appliquées pour l'analyse de jeux de données RADARSAT-1 antérieurement acquises en mode fin et en mode ScanSAR étroit B sur des navires et validées d'après des données du AIS Live.

Résultats: Pour chaque signature de navire validée, plusieurs mesures ont été calculées au moyen de l'outil VUSAR d'analyse d'images, dont les statistiques sur le fouillis d'échos, la section efficace en radar (RCS) de chaque navire et la longueur de la signature du navire. Ces mesures ont été évaluées en termes de polarisation, d'angle d'incidence local, de longueur validée du navire, du rapport cible sur fouillis et d'angle d'aspect du navire. On a relevé ce qui suit :

- le fouillis d'échos de l'océan en polarisation orthogonale est au plancher de bruit de l'ASAR de l'Envisat de sorte que toute mesure du contraste de cible serait établie par rapport au plancher de bruit de l'instrument plutôt que par rapport au fouillis d'échos de l'océan;
- le fouillis d'échos d'arrière-plan de l'océan peut être caractérisé comme présentant une distribution K;
- pour les cibles que sont les navires, les RCS totales en HH et en VV sont comparables alors que la RCS totale en polarisation orthogonale est d'environ 10 dB inférieure à la RCS totale en copolarisation; des modèles de la RCS totale en fonction de la longueur du navire sont fournis;
- en copolarisation, le contraste des navires cibles augmente lorsque augmente l'angle d'incidence alors qu'en polarisation orthogonale le contraste est plus ou moins indépendant de l'angle d'incidence; le contraste des navires cibles en copolarisation est plus grand en polarisation orthogonale si l'angle d'incidence est inférieur à 33°;
- la variabilité de la RCS totale a été modélisée avec succès en ajustant la RCS totale normalisée à plusieurs fonctions de distribution de probabilités bien connues; la variabilité de la RCS est moindre pour les signatures de navires en polarisation orthogonale;

- la longueur de la signature de navire correspondait avec la longueur validée des navires à 60,1 % en copolarisation et à 71,5 % en polarisation orthogonale; en copolarisation, le taux de sous-estimation de la longueur des navires est plus élevé; en polarisation orthogonale, le taux de surestimation de la longueur des navires est plus élevé; il y a tendance à davantage de surestimation de la longueur des navires pour les navires en déplacement en azimut;
- sur le canal de polarisation orthogonale les signatures de sillages de navires s'apparente aux signatures de navires n'ayant pas subi de décalage en azimut, comme c'Est le cas pour la signature du navire elle-même; ces signatures se manifestent fréquemment et peuvent être attribuables à la diffusion engendrée par les vagues soulevées à l'étrave du navire.

Importance: Le jeu de données décrit est très riche et a fourni de nouvelles observations et perspectives sur la détectabilité des navires par RSO. Ces résultats pourraient être importants pour la conception de futurs modes ou missions RSO et pourraient être utilisés pour l'amélioration du rendement des logiciels de détection de navires.

L'utilisation des données du SIA pour la validation des signatures de navires est une méthode éprouvée qui devrait être utilisée pour l'élaboration de modèles de détection de navires dans le cadre d'autres missions comme les TerraSAR-X et Cosmos-Skymed. Le fait de concentrer les travaux sur les à grande densité d'activité maritime fournirait un important jeu de navires cibles validés pour chaque image acquise.

Table of contents

List of figures

List of tables

Acknowledgements

We thank Dr. J.K.E. (Jake) Tunaley (Polar Epsilon R&D Manager) for his interest in and support of this work. Dr. R. English (DRDC Ottawa) helped with analysis of the AISLive data. The Envisat ASAR images discussed in this document were obtained via Envisat Announcement of Opportunity (AO) Project #255, and are copyright European Space Agency, 2006 and 2007. We thank Ryan English (DRDC Ottawa), Bob Hawkins (Canada Centre for Remote Sensing), Peter Meadows (BAE Systems), and Betlem Rosisch (European Space Agency) for helpful discussions.

1 Introduction

Ships appear in synthetic aperture radar (SAR) ocean imagery as bright targets against the ocean clutter background. Ship signature characterization in RADARSAT-1 (R-1) and Envisat Advanced SAR (ASAR) imagery can improve automatic ship detection algorithms, identify signature metrics for ship classification, and provide information for predicting the ship detection performance of future SAR systems.

Recently, R-1 (C-band, HH polarization) Fine mode and ScanSAR Narrow B (SCNB) mode data sets were successfully acquired, along with AISLive (www.aislive.com) data that were used for ship signature validation [1], [2], [3]. This document describes the extension of the R-1 activity to include other polarizations by using the Envisat ASAR (C-band) Alternating Polarization (AP) mode. This work provides new insight to the impact of polarization choices on ship detection.

The available data sets and a high-level summary of the analysis results from all trials have already been described elsewhere [4].

Envisat ASAR AP mode data acquisition over the Strait of Dover and the Strait of Gibraltar, two high-density shipping regions with AISLive coverage, commenced in mid-November 2006 and finished by mid-February 2007. A total of 42 alternating polarization (AP) mode images representing all seven ASAR beams (i.e., IS1 through IS7, represented the smallest to largest incidence angles) and including all three available dual polarization configurations (i.e., HH/HV, VV/VH, and HH/VV) were ordered, along with 42 time-coincident pairs of AISLive snapshot data sets bracketing each ASAR image acquisition time.

The Envisat ASAR images were obtained through European Space Agency (ESA) Announcement of Opportunity (AO) project #255 (P.W. Vachon, Principle Investigator). The images were obtained from ESA as radiometrically calibrated, precision 16-bit products. Some of the products were obtained via the Envisat Rolling Archive within a few days of acquisition. Others were obtained via CD-ROM.

Of the 42 images ordered, 35 ASAR images were eventually received. The remaining 7 images were not acquired due to programming conflicts or technical issues with the satellite operation. All of the corresponding AISLive data sets were received via email within a few days of data acquisition.

The ships present in the 35 acquisitions, as reported by AISLive, were validated through the Internet Ships Register (ISR) (www.ships-register.com). The validation procedure consists of matching the AISLive ship position information with the closest SAR target signature, and performing a handshake via the International Maritime Organization (IMO) number to access the definitive ISR database ship specifications (i.e., the ship length).

Processing of the AISLive data was carried out as described in [3] to establish the AIS-projected ship position at the Envisat pass time, the AIS-predicted ship position that accounts for azimuth shifting of the AIS-projected position, the actual ship signature position, the ship radar cross section (RCS), and other ship signature metrics. The analysis methods are similar to those used to analyze the previously acquired R-1 Fine and SCNB data sets.

Section 2 contains a summary of the ASAR and validation data sets; Section 3 describes the properties of the background clutter against which the ship signatures appear; Section 4 addresses the ship RCS and related contrast measures; Section 5 models the variability of the observed ship RCS; Section 6 compares the ship signature length with the validated ship length; and. Section 7 contains some examples of ship wakes observed in the cross-polarization channel data.

2 Data summary

The ASAR data were ordered using Earthnet OnLine Interactive (EOLI), a GUI-based tool that provides access to the online ESA catalogues of EO products. AISLive data sets were ordered and received via e-mail from Lloyd's Register-Fairplay once the ASAR orders were confirmed.

Table 1 summarizes the ASAR/AISLive acquisition parameters. A red row indicates an ASAR programming conflict while a magenta row indicates that beam IS5 was inoperable and that no ASAR data for that beam mode and polarization combination were acquired. Each data set consists of one image and two AISLive snapshots, one acquired before the ASAR pass time and one acquired after the ASAR pass time, collected nominally 3 minutes apart.

The basic statistics for the number of validated ships in the 4 linear polarizations are shown in Table 2. The various parameters in the table are described elsewhere [3]. The total number of ships available for each polarization state has been highlighted in yellow and represents high confidence matches between the AIS-predicted location and the target signature location.

The AISLive-reported ship length was verified against the ISR database ship length via a scatterplot, as shown in Figure 1. There are several different measures of ship length (e.g., length overall, waterline length, scantling length). Therefore, an error was defined in the verification process as a difference between the AISLive-reported length and the ISR database length overall of 30% or more. The error rate is close to 10.5%, which is slightly larger than, but generally consistent with, the error rate seen in the previous AISLive data sets. Ship length errors include the ship length reported in feet rather than meters, ship width or some other measure appearing in the ship length field, and most frequently, a reported ship length of zero. In a few cases, a ship length was not available from the ISR database.

Histograms of the separation distance between the AIS-predicted position and the target signature position are shown in Figure 2, with one histogram presented for each polarization. The mean (≈ 150 m) and standard deviation (≈ 75 m), as shown in the title of each sub-plot, are similar for each polarization.

Histograms of the ship lengths extracted from the ISR Database for the validated ships in each linear polarization are shown in Figure 3. The mean (≈ 150 m) and standard deviation (≈ 60 m) are similar for each polarization. Note that the mean distance between the AIS-prediction position and the target signature position is about the same as the mean ship size the database. This reflects good performance in the use of AIS for ship signature validation.

Histograms of the estimated total RCS for the ships in each polarization are shown in Figure 4. As with the R-1 data considered previously, there is a very wide range of radar cross sections observed, with the cross-polarization RCS being systematically smaller than the co-polarization RCS.

Validated ships are not identically visible in each available channel of AP mode data. This is especially true for smaller incidence angles. Examples of recognizable VH ship signatures versus undetectable VV ship signatures at near incidence angles are shown in Figure 5. Similarly, range-ward transects of normalized radar cross section at small and large incidence angles are shown in

Figure 6. Note how the target contrast becomes larger for larger incidence angles, especially for co-polarization at low incidence angle, which is dominated by clutter.

Table 1: ASAR/AISLive acquisition parameters.

Site	*Swath*	*Pol*	*Orbit*	*Track*	*Pass*	*Date*	*ASAR StartTime*	*ASAR StopTime*	*ASAR CentreTime*	*AIS Snap1*	*AIS Snap2*
Dover	IS1	HH/HV	24761	158	A	24-Nov-06	21:27:36	21:28:51	21:28:13	21:27:13	21:30:13
		VV/VH	24990	387	A	10-Dec-06	21:24:45	21:25:01	21:24:53	21:23:53	21:26:55
		HH/VV	25656	51	D	26-Jan-07	10:25:15	10:25:30	10:25:22	10:24:23	10:27:23
Dover	IS2	HH/HV	25885	280	D	11-Feb-07	10:22:24	10:22:39	10:22:31	10:21:31	10:24:31
		VV/VH	25534	430	A	17-Jan-07	21:30:25	21:30:40	21:30:32	21:29:33	21:32:33
		HH/VV	25384	280	D	7-Jan-07	10:22:24	10:22:40	10:22:32	10:21:33	10:24:33
Dover	IS3	HH/HV	24804	201	A	27-Nov-06	21:33:18	21:33:33	21:33:25	21:32:26	21:35:25
		VV/VH	25805	201	A	5-Feb-07	21:33:16	21:33:31	21:33:23	21:32:23	21:35:24
		HH/VV	25305	201	A	1-Jan-07	21:33:17	21:33:32	21:33:24	21:32:24	21:35:24
Dover	IS4	HH/HV	25849	244	A	8-Feb-07	21:39:00	21:39:15	21:39:07	21:38:08	21:41:10
		VV/VH	25348	244	A	4-Jan-07	21:38:59	21:39:14	21:39:07	21:38:06	21:41:06
		HH/VV	25076	473	A	16-Dec-06	21:36:09	21:36:24	21:36:16	21:35:16	21:38:16
Dover	IS5	HH/HV	25620	15	A	23-Jan-07	21:41:51	21:42:06	21:41:59		
		VV/VH	25255	151	D	29-Dec-06	10:05:19	10:05:34	10:05:26		
		HH/VV	25119	15	A	19-Dec-06	21:41:51	21:42:06	21:41:59		
Dover	IS6	HH/HV	25162	58	A	22-Dec-06	21:47:33	21:47:48	21:47:41	21:46:41	21:49:41
		VV/VH	25663	58	A	26-Jan-07	21:47:31	21:47:46	21:47:38	21:46:40	21:49:38
		HH/VV	24661	58	A	17-Nov-06	21:47:33	21:47:48	21:47:41	21:46:12	21:49:12
Dover	IS7	HH/HV	25434	330	A	10-Jan-07	21:50:24	21:50:39	21:50:32	21:49:32	21:52:32
		VV/VH	24933	330	A	6-Dec-06	21:50:24	21:50:40	21:50:32	21:49:32	21:52:32
		HH/VV	25935	330	A	14-Feb-07	21:50:25	21:50:40	21:50:32	21:49:32	21:52:32
Gibraltar	IS1	HH/HV	24969	366	D	9-Dec-06	10:38:07	10:38:22	10:38:15	10:37:16	10:40:15
		VV/VH	25334	230	A	3-Jan-07	22:06:30	22:06:45	22:06:37	22:05:37	22:08:37
		HH/VV	25198	94	D	25-Dec-06	10:35:16	10:35:32	10:35:24	10:34:25	10:37:25
Gibraltar	IS2	HH/HV	24926	323	D	6-Dec-06	10:32:26	10:32:41	10:32:34	10:31:36	10:34:34
		VV/VH	25105	1	A	18-Dec-06	22:09:20	22:09:35	22:09:28	22:08:28	22:11:28
		HH/VV	25427	323	D	10-Jan-07	10:32:26	10:32:41	10:32:34	10:31:34	10:34:34
Gibraltar	IS3	HH/HV	25155	51	D	22-Dec-06	10:29:35	10:29:51	10:29:43	10:28:45	10:31:43
		VV/VH	25656	51	D	26-Jan-07	10:29:36	10:29:51	10:29:43	10:28:43	10:31:43
		HH/VV	25148	44	A	21-Dec-06	22:15:01	22:15:16	22:15:08	22:14:18	22:17:09
Gibraltar	IS4	HH/HV	24919	316	A	5-Dec-06	22:17:52	22:18:07	22:17:59	22:17:02	22:19:59
		VV/VH	25420	316	A	9-Jan-07	22:17:52	22:18:07	22:17:59	22:16:59	22:19:59
		HH/VV	25384	280	D	7-Jan-07	10:26:45	10:27:00	10:26:52	10:25:53	10:28:53
Gibraltar	IS5	HH/HV	25191	87	A	24-Dec-06	22:20:43	22:20:58	22:20:50	22:19:50	22:22:50
		VV/VH	25112	8	D	19-Dec-06	10:23:54	10:24:09	10:24:01	10:23:02	10:26:02
		HH/VV	25692	87	A	28-Jan-07	22:20:43	22:20:58	22:20:50		
Gibraltar	IS6	HH/HV	24962	359	A	8-Dec-06	22:23:33	22:23:48	22:23:40	22:22:40	22:25:41
		VV/VH	25341	237	D	4-Jan-07	10:21:04	10:21:19	10:21:11	10:20:11	10:23:11
		HH/VV	25842	237	D	8-Feb-07	10:21:04	10:21:19	10:21:11	10:20:11	10:23:07
Gibraltar	IS7	HH/HV	25069	466	D	16-Dec-06	10:18:13	10:18:28	10:18:20	10:17:22	10:20:20
		VV/VH	25735	130	A	31-Jan-07	22:26:24	22:26:39	22:26:32	22:25:32	22:28:33
		HH/VV	25234	130	A	27-Dec-06	22:26:24	22:26:39	22:26:32	22:25:33	22:28:34

Table 2: Statistics for validated ship signatures.

Polarization	=	HH
Total #AIS records within ASAR coverage	=	2038
# AIS records with IMO < 0	=	0
# AIS records with IMO = 0	=	53
# AIS records with IMO = 1	=	0
# AIS ships landmasked	=	944
# AIS ships portmasked	=	174
# AIS ships at image edge	=	19
# AIS ships with airballs	=	31
# AIS ships with multitargs detected in target subscene	=	25
# AIS ships with multiple AIS hits at same target location	=	5
# AIS ships with no significant target signature	=	78
# counts where no AIS to ISR match occurred	=	20
# aistargtotalrcs<=0	=	0
# ISR lengths found <= 0 meters	=	0
# AIS ships with signiftargsig > search radius of 400m	=	17
# AIS ships with signiftargsig <= search radius of 400m	=	672
Polarization	=	VV
Total #AIS records within ASAR coverage	=	1921
# AIS records with IMO < 0	=	0
# AIS records with IMO = 0	=	38
# AIS records with IMO = 1	=	0
# AIS ships landmasked	=	862
# AIS ships portmasked	=	164
# AIS ships at image edge	=	19
# AIS ships with airballs	=	30
# AIS ships with multitargs detected in target subscene	=	22
# AIS ships with multiple AIS hits at same target location	=	3
# AIS ships with no significant target signature	=	84
# counts where no AIS to ISR match occurred	=	30
# aistargtotalrcs<=0	=	0
# ISR lengths found <= 0 meters	=	1
# AIS ships with signiftargsig > search radius of 400m	=	10
# AIS ships with signiftargsig <= search radius of 400m	=	658
Polarization	=	HV
Total #AIS records within ASAR coverage	=	1083
# AIS records with IMO < 0	=	0
# AIS records with IMO = 0	=	28
# AIS records with IMO = 1	=	0
# AIS ships landmasked	=	506
# AIS ships portmasked	=	86
# AIS ships at image edge	=	6
# AIS ships with airballs	=	19
# AIS ships with multitargs detected in target subscene	=	13
# AIS ships with multiple AIS hits at same target location	=	2
# AIS ships with no significant target signature	=	15
# counts where no AIS to ISR match occurred	=	11
# aistargtotalrcs<=0	=	0
# ISR lengths found <= 0 meters	=	0
# AIS ships with signiftargsig > search radius of 400m	=	10
# AIS ships with signiftargsig <= search radius of 400m	=	387
Polarization	=	VH
Total #AIS records within ASAR coverage	=	966
# AIS records with IMO < 0	=	0
# AIS records with IMO = 0	=	13
# AIS records with IMO = 1	=	0
# AIS ships landmasked	=	424
# AIS ships portmasked	=	76
# AIS ships at image edge	=	6
# AIS ships with airballs	=	18
# AIS ships with multitargs detected in target subscene	=	6
# AIS ships with multiple AIS hits at same target location	=	0
# AIS ships with no significant target signature	=	6
# counts where no AIS to ISR match occurred	=	18
# aistargtotalrcs<=0	=	0
# ISR lengths found <= 0 meters	=	0
# AIS ships with signiftargsig > search radius of 400m	=	3
# AIS ships with signiftargsig <= search radius of 400m	=	396

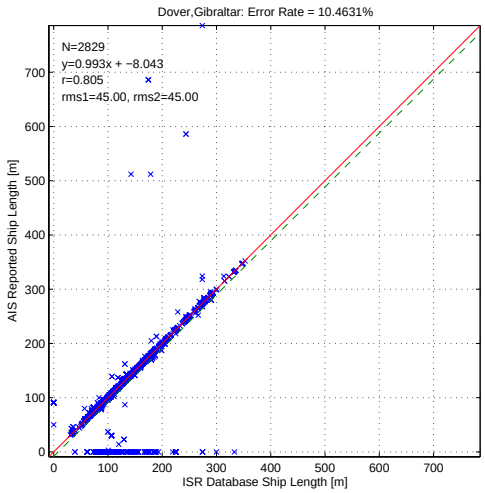

Figure 1: Scatterplot of AISLive-reported and ISR Database-validated ship lengths.

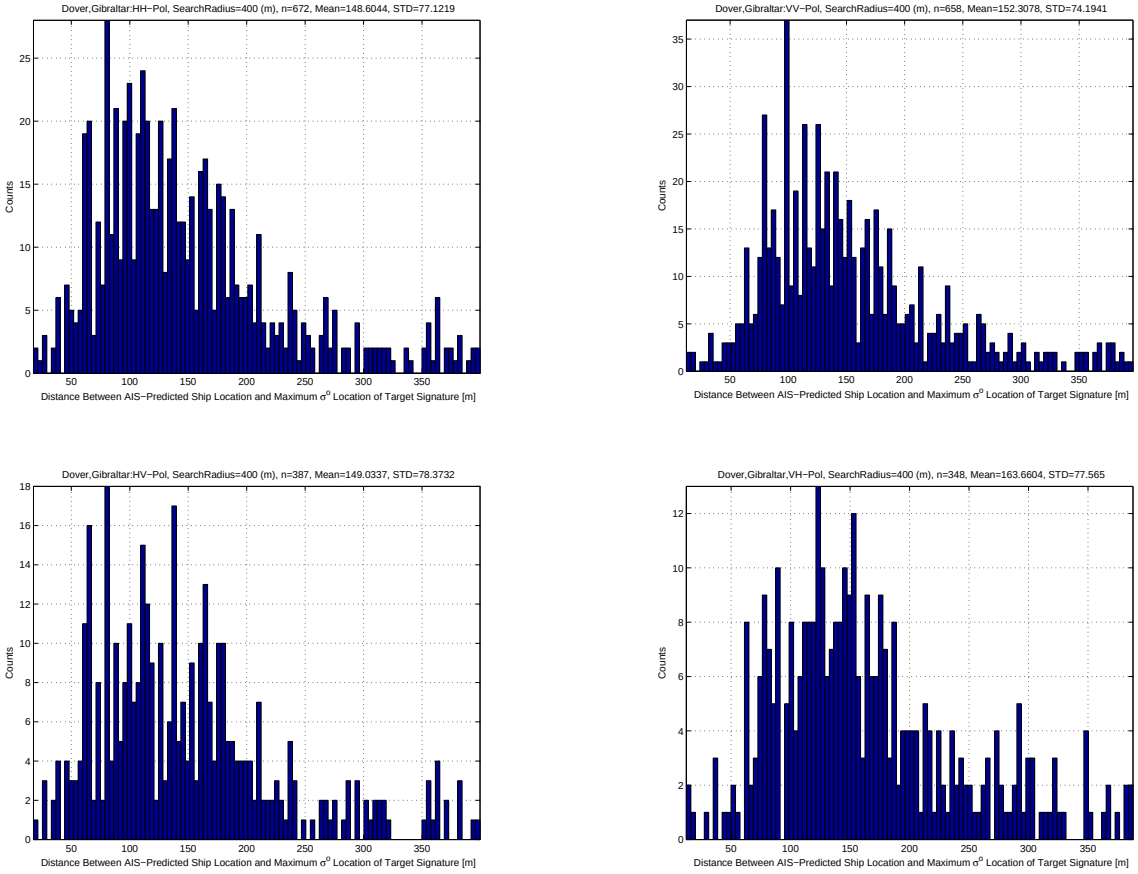

Figure 2: Histograms of the distance between the AIS-predicted ship position and the SAR signature position for each linear polarization.

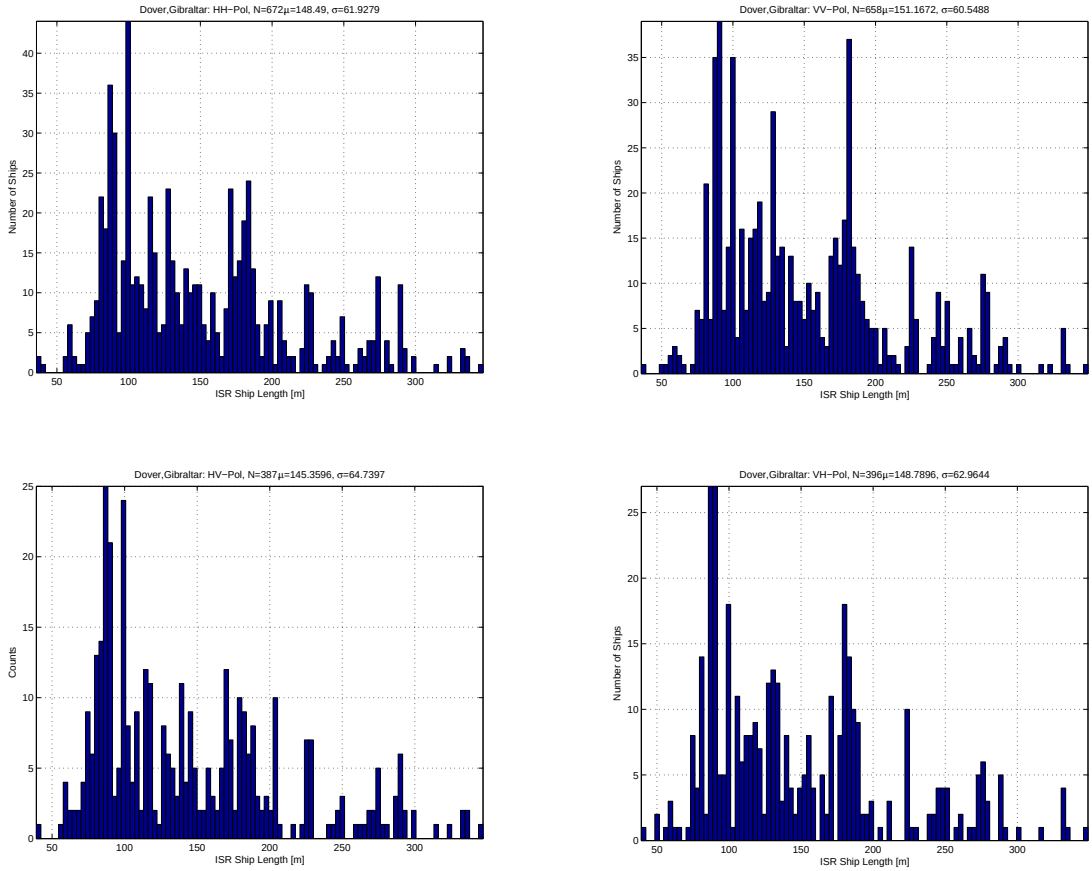

Figure 3: Histograms of ISR Database validated ship lengths for each linear polarization.

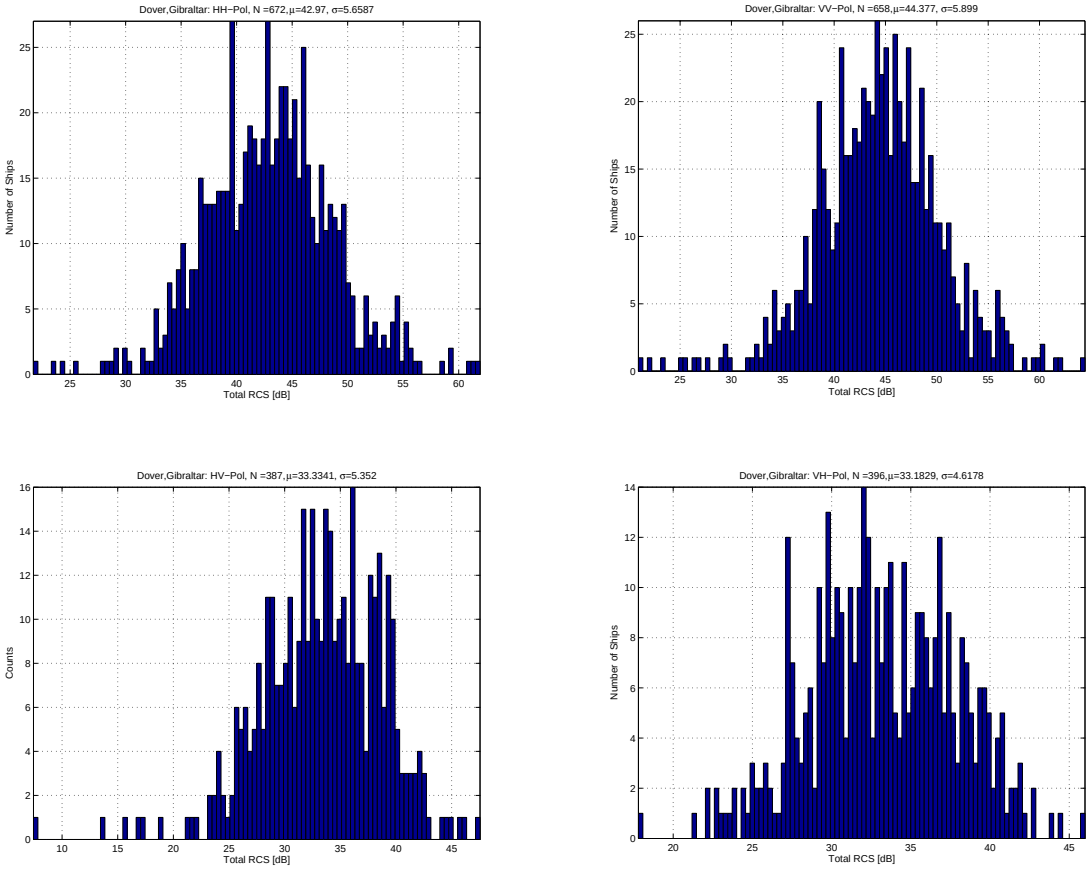

Figure 4: Histograms of total RCS for the validated ships for each linear polarization.

Gibraltar, 2007-01-03, IS1, VV-pol

Gibraltar, 2007-01-03, IS1, VH-pol

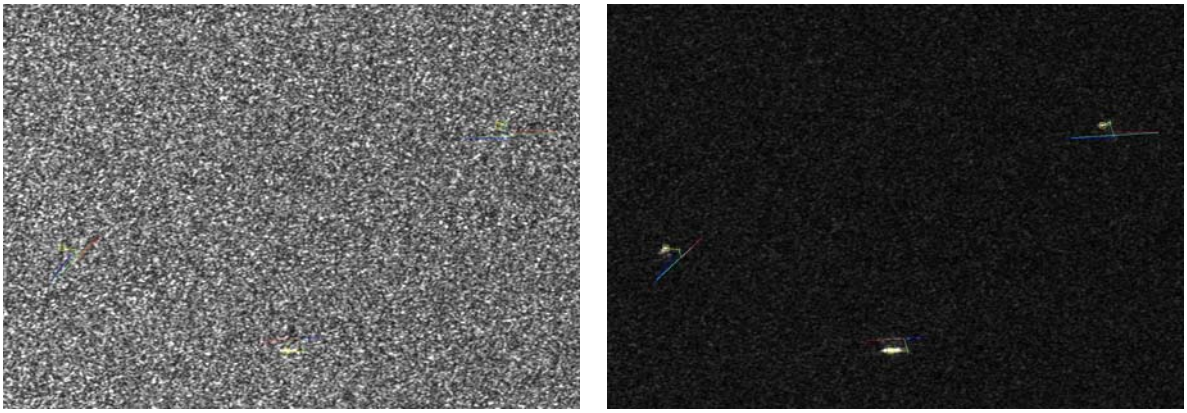

Figure 5: An example of VV and VH images of ships at low incidence angles.

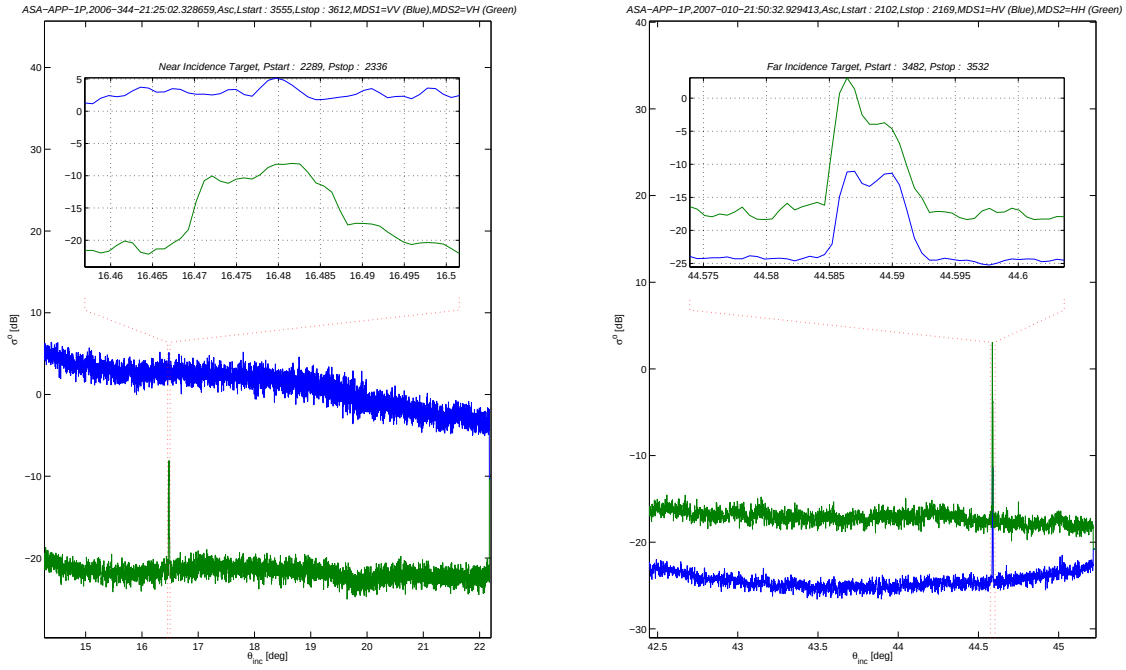

Figure 6: Range-ward transects of normalized radar cross section through ship targets at near (left) and far (right) incidence angles.

3 Ocean clutter

To better understand the clutter against which the ship signature is measured, the clutter estimates derived during the ship signature analysis were plotted as a function of incidence angle (θ_{inc}) for co-polarizations in Figure 7 and for cross-polarizations in Figure 8. Also plotted are Envisat ASAR noise floor estimates, expressed as noise-equivalent-sigma-zero [5].

These plots illustrate the following: the clutter level decreases with increasing incidence angle for co-polarization, sometimes reaching the instrument noise floor; VV clutter levels are generally higher than HH clutter levels; the cross-polarization clutter is normally at the noise floor, except for the smallest incidence angles in the data set at which there could be as much as a few dB of clutter signal.

In ship detection systems, the background clutter level is generally modelled as K-distributed noise. We represent the clutter variability by plotting in Figure 9 the mean-squared to variance ratio (MSVR), a measure of the number of statistically independent looks for a Gaussian scene, as a function of the incidence angle and polarization. The upper limit of this parameter should be close to the number of independent looks, which is range-dependent for Envisat ASAR since the ground range resolution is held more-or-less constant with range and the extra available spatial resolution is converted to radiometric resolution. Also plotted are nominal values of the equivalent number of looks (ENL) for each beam mode [5].

Smaller values of MSVR are related to higher clutter variability, indicating non-Gaussian behaviour that may be characterized through use of a K-distributed clutter model. One approach to estimating the K-distribution order parameter uses the observed MSVR and the ENL [6]. Histograms of the order parameter are shown in Figure 10. For co-polarization, 66.5% of the cases have a K-distribution order parameter that is smaller than 100, representing cases with a departure from Gaussian statistics. That is, the co-polarization clutter is generally non-Gaussian in nature. On the other hand, for cross-polarization, only 18.6% of the cases have a K-distribution order parameter that is smaller than 100. That is, the cross-polarization clutter is generally Gaussian in nature. Indeed, the ASAR cross-polarization clutter is generally just the instrument noise floor.

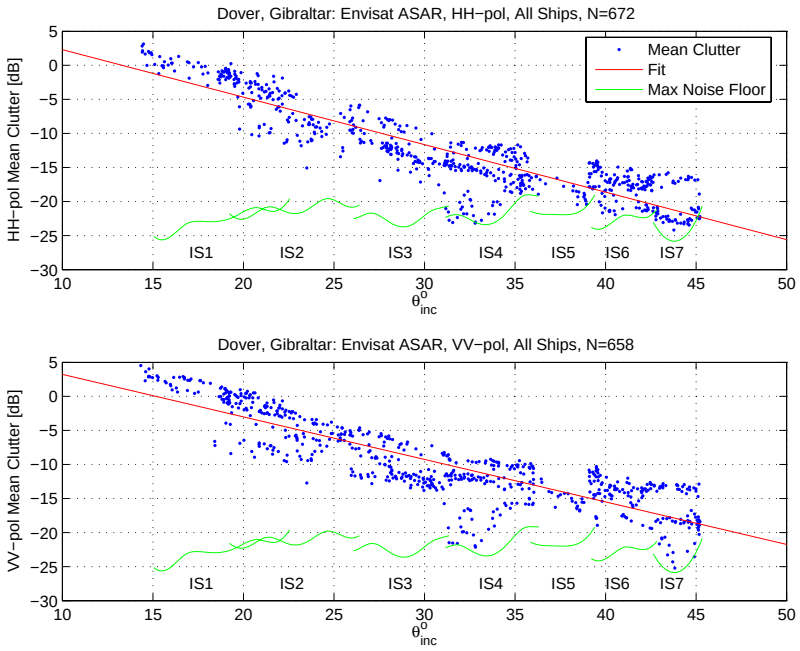

Figure 7: Mean co-polarization ocean clutter as a function of incidence angle for each ship analyzed.

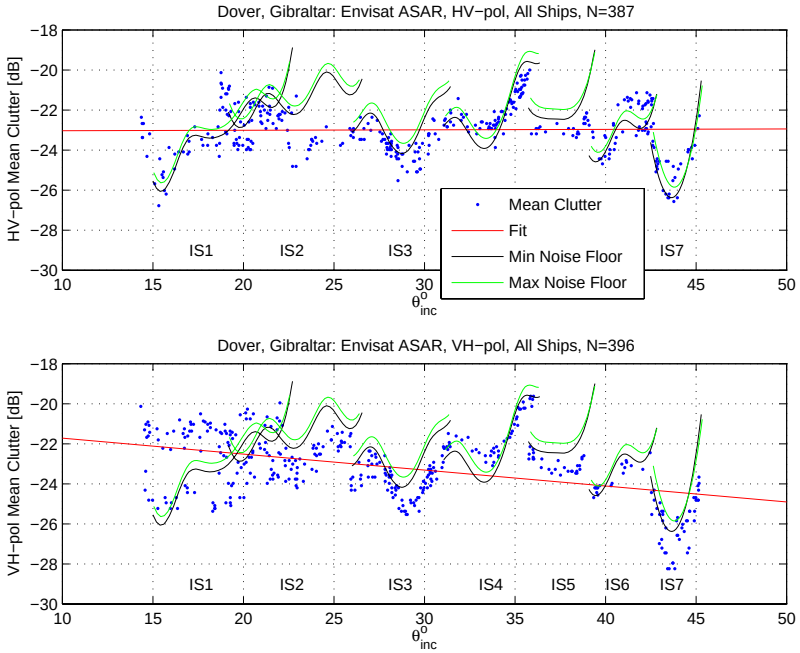

Figure 8: Mean cross-polarization ocean clutter as a function of incidence angle for each ship analyzed.

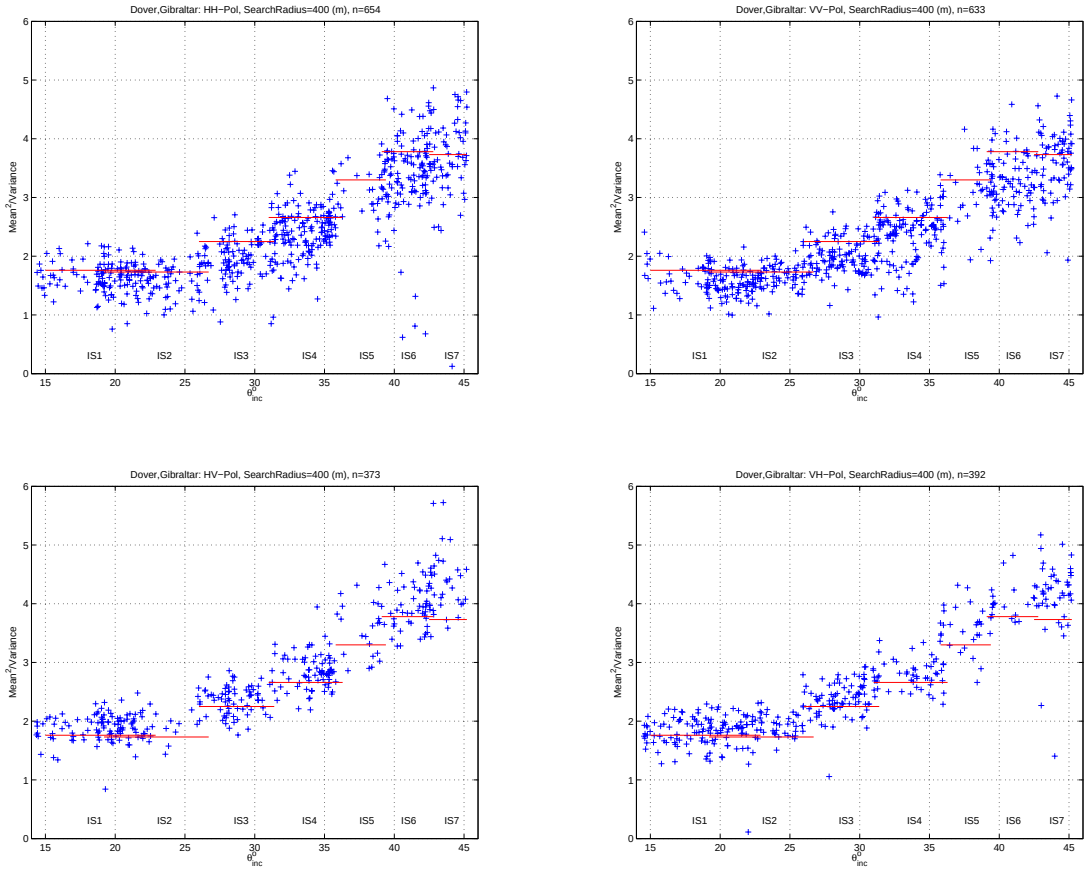

Figure 9: Mean-squared to Variance Ratio as a function of incidence angle for the ocean clutter associated with each ship analyzed for each linear polarization. The red lines indicate the ENL for each ASAR beam mode.

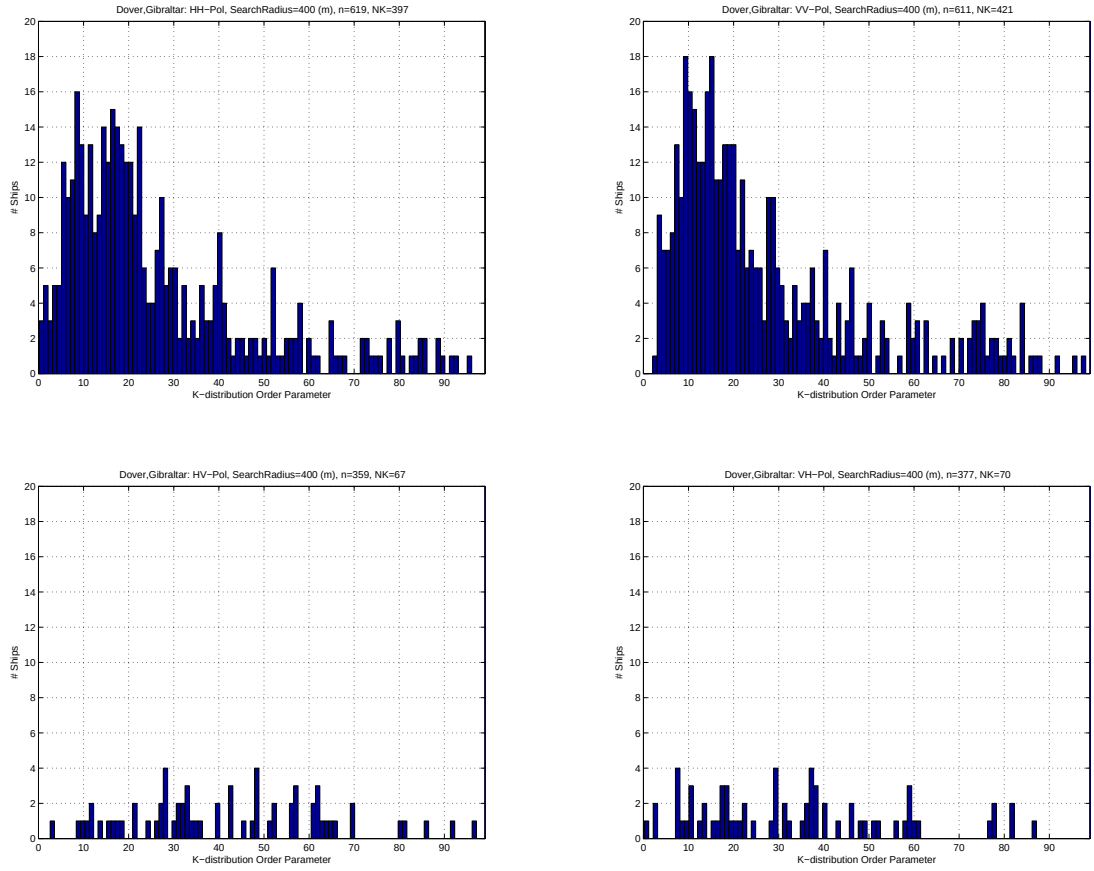

Figure 10: Histograms of the K-distribution order parameter for the ocean clutter associated with each ship analyzed and for each linear polarization.

4 Target RCS and contrast metrics

In developing target contrast metrics, we considered three target RCS metrics: *Total RCS, Peak Region RCS,* and *Segmented Region RCS*. All are based upon a 64 by 64 pixels analysis subscene that is centred on the peak σ° (i.e., normalized radar cross section) value. The 16-bit ESA products considered are radiometrically calibrated and provide σ° directly. Note that ship target saturation was not observed in any of the datasets.

Total RCS is the integration of σ° over the entire target subscene with the mean clutter, based upon clutter estimates from the four 16 by 16 pixels corners of the analysis subscene, removed.

Peak Region RCS (PR_{RCS}) is the integration of σ° over the peak region with the mean clutter removed. The peak region is defined to be twice the 3 dB width of the target signature centered on the maximum σ° location in the target subscene (this is a standard Envisat ASAR calibration team definition).

Segmented Region RCS (SR_{RCS}) is the integration of σ° over a segmented target region with the mean clutter removed. A pixel within the target subscene is included in the segmented target region if:

$$\sigma^\circ > \text{mean}\left(\sigma^\circ_{clut}\right) + 5\,\text{std}\left(\sigma^\circ_{clut}\right),$$

where mean and std are the average value and the standard deviation operations. The segmented region can be "cleaned-up" by using sequential erosion and dilation morphological operations, which is useful for target length estimation, but generally has little impact on the estimated SR_{RCS}.

Some possible contrast metrics include: *Peak-to-Clutter Ratio, Peak Region RCS-to-Clutter Ratio,* and the *Segmented Region RCS-to-Clutter Ratio*.

Peak-to-Clutter Ratio is defined as $\sigma^\circ_{\max} / \text{mean}\left(\sigma^\circ_{clut}\right)$, where $\sigma^\circ_{\max}$ is the target subscene maximum σ° value.

Peak Region RCS-to-Clutter Ratio is defined as $\left[PR_{RCS} / \text{mean}\left(\sigma^\circ_{clut}\right)\right] / PR_{area}$ where PR_{area} is the *Peak Region* area in square meters;

Segmented Region RCS-to-Clutter Ratio is equal to $\left[SR_{RCS} / \text{mean}\left(\sigma^\circ_{clut}\right)\right] / SR_{area}$ where SR_{area} is the *Segmented Region* area in square meters.

Scatterplots of the peak region RCS and the total RCS are shown in Figure 11. In general, the peak region RCS underestimates the total RCS. The peak region RCS is not appropriate if the signature contains several bright components since only the largest is measured. Discrepancies of up to 15 dB are noted.

Scatterplots of the segmented region RCS and the total RCS are shown in Figure 12. These RCS measures are generally in good agreement, especially for larger RCS values. For contrast measures we will generally focus on using the segmented region RCS since a target area estimate is required for the contrast metric.

Scatterplots of the peak-to-clutter ratio and the peak region RCS-to-clutter ratio are shown in Figure 13. These contrast metrics are well-correlated for larger contrast values.

Scatterplots of the peak-to-clutter ratio and the segmented region RCS-to-clutter ratio are shown in Figure 14. These contrast metrics are reasonably well correlated, but we feel that the segmented region RCS-to-clutter ratio is a better measure since it includes an RCS that is closer to the total RCS. For completeness, all of the contrast metrics are included in subsequent analysis.

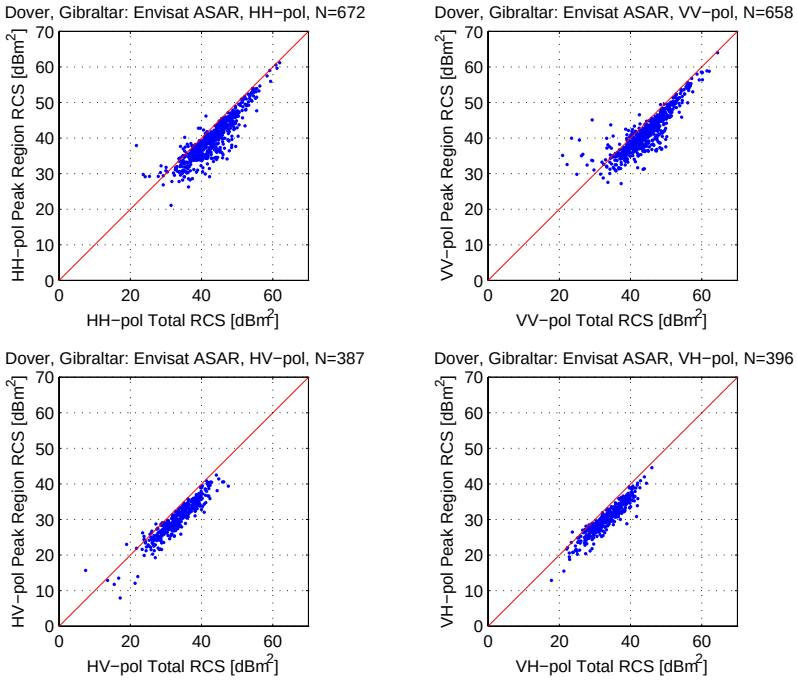

Figure 11: Scatterplots of peak region RCS and total RCS for each linear polarization.

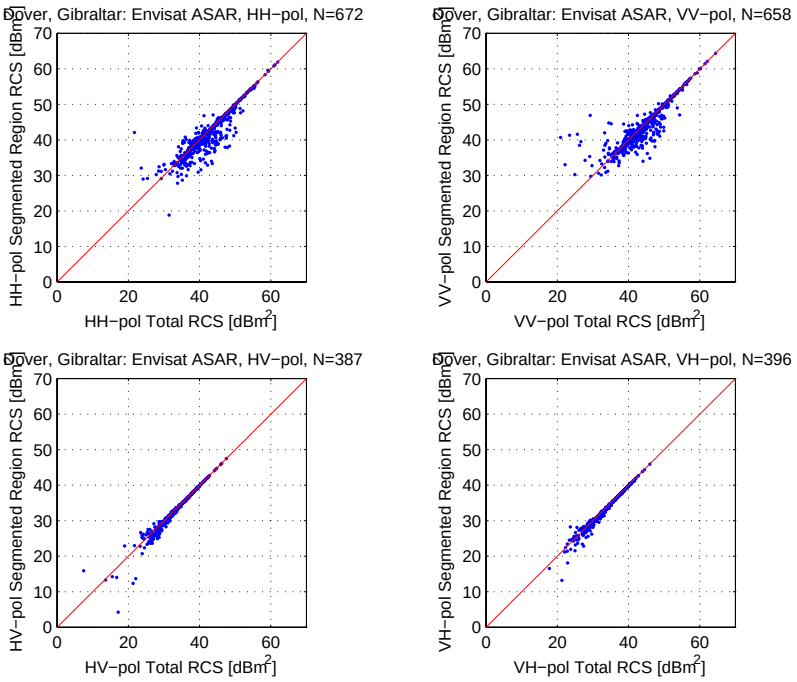

Figure 12: Scatterplots of segmented region RCS and total RCS for each linear polarization.

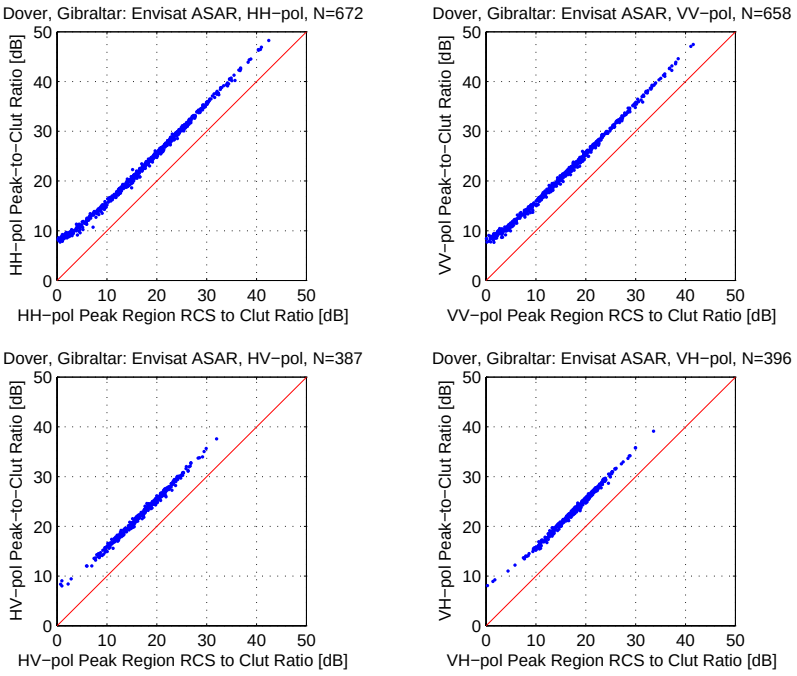

Figure 13: Scatterplots of peak-to-clutter ratio and peak region RCS-to-clutter ratio for each linear polarization.

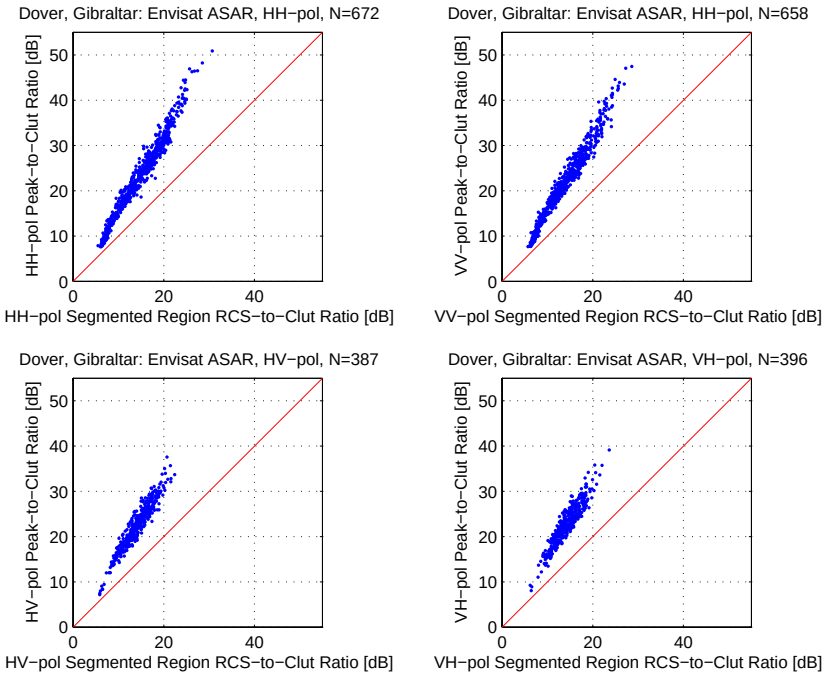

Figure 14: Scatterplots of peak-to-clutter ratio and segmented region RCS-to-clutter ratio for each linear polarization.

4.1 Total RCS

Scatterplots of the total RCS versus the ISR Database validated ship length for each polarization are shown in Figure 15. In each case, a simple regression of the RCS as a function of the ship length has been carried out to show the general trend in the data; the model coefficients are included in the title of each sub-plot. For comparison, previous such model fits to the R-1 Fine mode [2] and SCNB [3] data are included on each plot. We see that the co-polarization data are very similar to the R-1 data acquired at HH polarization, while the cross-polarization data are around 10 dB smaller, as observed previously with Environment Canada (EC) CV-580 C-band polarimetric SAR imagery of known ships [7].

Scatterplots of total RCS for co- and cross-polarization data (i.e., combined HH and VV data, and combined HV and VH data) are shown in Figure 16, along with the combined model fits. At this stage, we don't observe any obvious differences between the co-polarization channels (i.e., between HH and VV) or between the cross-polarization channels (i.e., between VH and HV).

Table 3 summarizes the ASAR total RCS regression fit parameters where σ is a function of the ship length (L). The R-1 total RCS regression fit parameters are also included for both the Fine and SCNB mode datasets.

Figure 17 shows the total RCS regression fits for the R-1 and ASAR data sets on the left, and the total RCS regression fits normalized by the RADARSAT Fine mode fit on the right. These plots illustrate that the co-polarization results agree among the various regression fits to within 2 dB, for all ship lengths. On the other hand, the cross-polarization ship RCS is about 10 dB smaller than the co-polarization ship RCS.

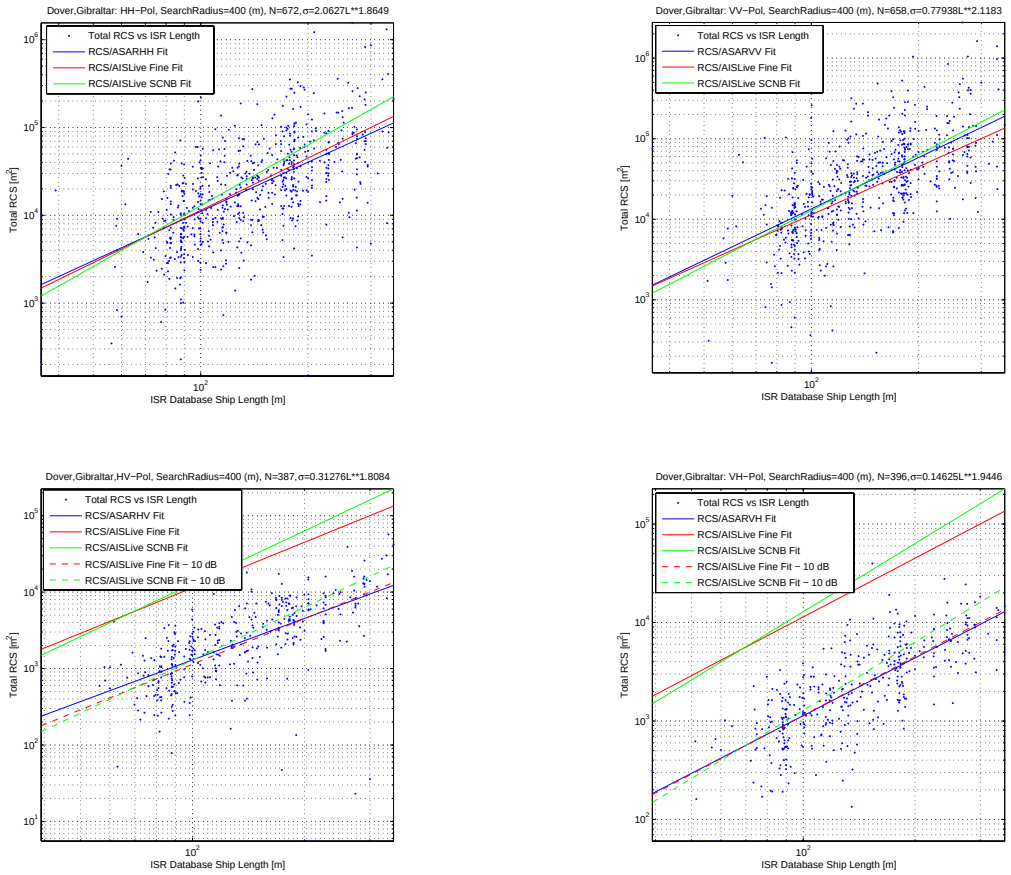

Figure 15: Scatterplots of total RCS and ISR Database validated ship length for each linear polarization.

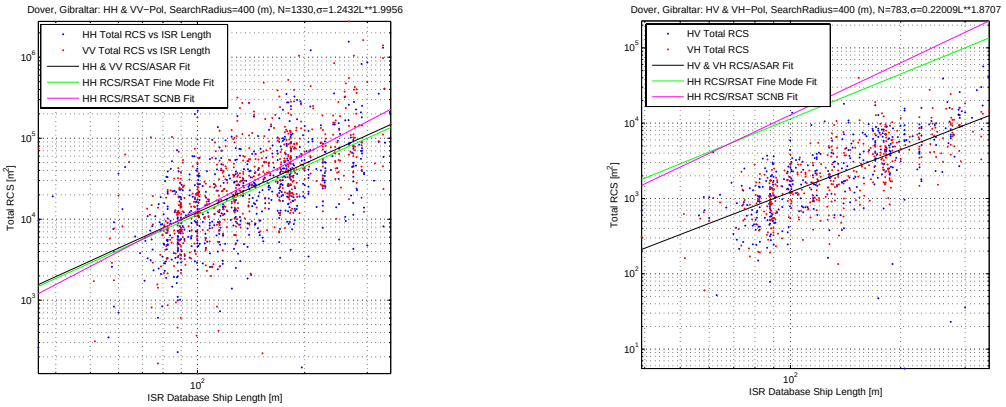

Figure 16: Scatterplots of total RCS and ISR Database validated ship length for co-polarization (left) and cross-polarization (right) data.

Table 3: Total RCS regression fit parameters.

	Regression Equation	**# Ships**
ASAR	$\sigma_{HH} = 2.0627 * \mathrm{L}^{1.8649}$	672
“	$\sigma_{VV} = 0.77938 * \mathrm{L}^{2.1183}$	658
“	$\sigma_{HV} = 0.31276 * \mathrm{L}^{1.8084}$	387
“	$\sigma_{VH} = 0.14625 * \mathrm{L}^{1.9446}$	396
“	$\sigma_{Co-pol} = 1.2432 * \mathrm{L}^{1.9956}$	1330
“	$\sigma_{Cross-pol} = 0.22009 * \mathrm{L}^{1.8707}$	783
R-1	$\sigma_{Fine} = 1.2499 * \mathrm{L}^{1.9798}$	399
“	$\sigma_{SCNB} = 0.32425 * \mathrm{L}^{2.2991}$	1805

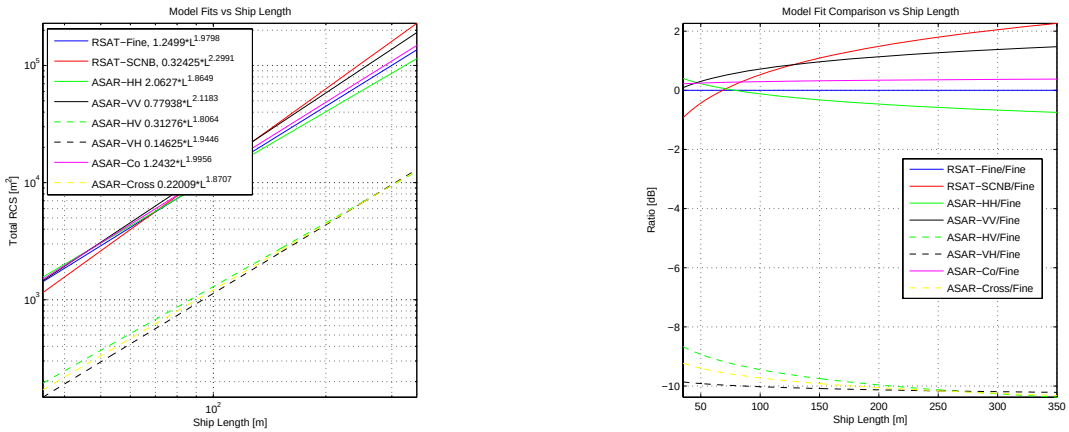

Figure 17: Total RCS regression fits for the R-1 and ASAR data sets (left) and the total RCS regression fits normalized by the R-1 Fine mode fit (right).

4.2 RCS and contrast metrics versus ship length

We now consider the extracted ship contrast metrics as a function of the validated ISR ship length. The three RCS metrics for co-polarization have been plotted in Figure 18 and for cross-polarization in Figure 19. In each case, the R-1 Fine and SCNB models were based on the total RCS.

The three contrast metrics for co-polarization are shown in Figure 20 and for cross-polarization in Figure 21. Included in the plots are linear fits to the observed data to show the general trend. The dependence on ship length is much clearer for the cross-polarization data, which is essentially measured against the instrument noise floor. It is apparent that the cross-polarization data have much less variability.

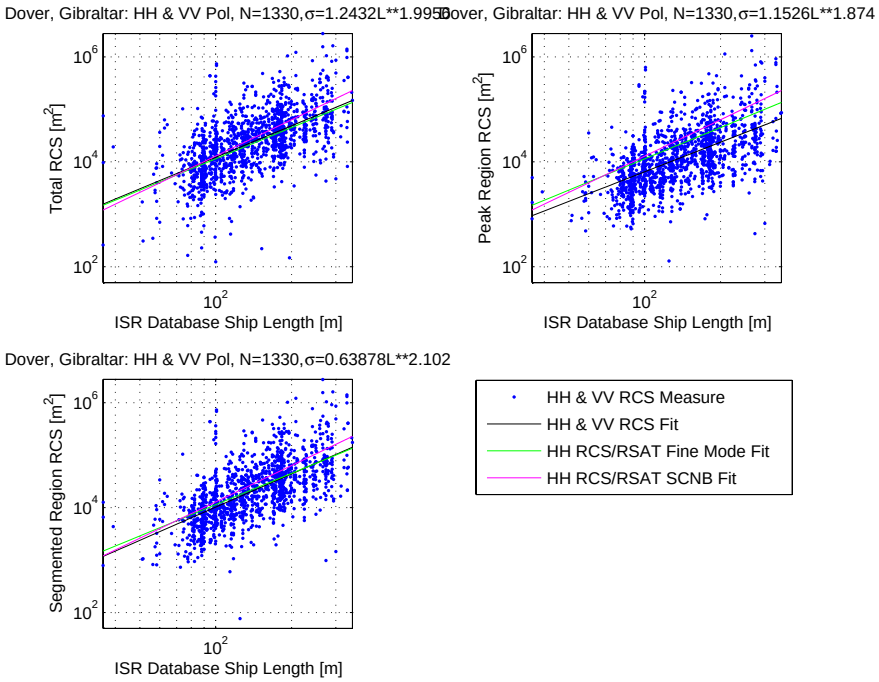

Figure 18: Scatterplots of RCS metrics for co-polarization versus validated ship length.

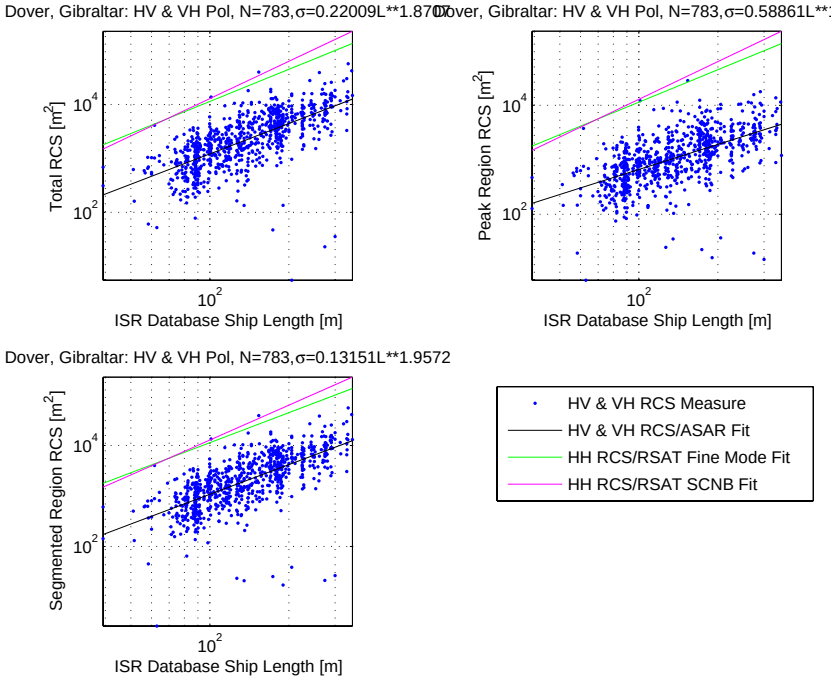

Figure 19: Scatterplots of RCS metrics for cross-polarization versus validated ship length.

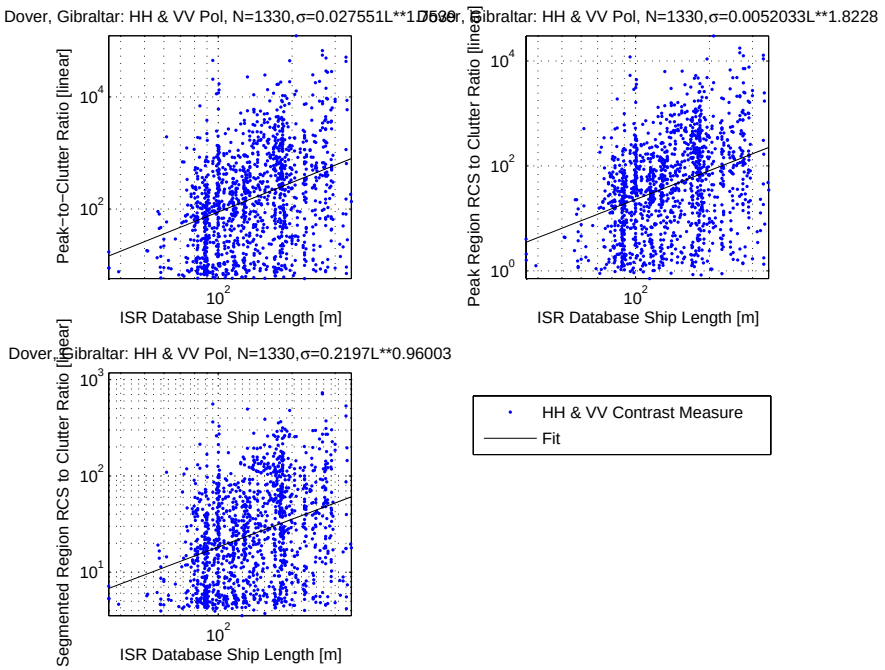

Figure 20: Scatterplots of contrast metrics for co-polarization versus validated ship length.

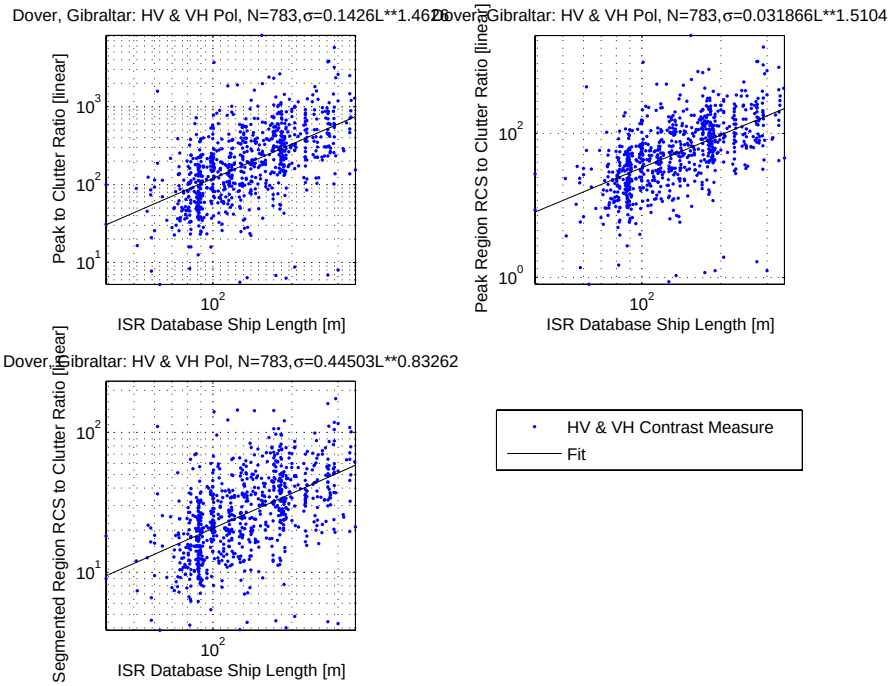

Figure 21: Scatterplots of contrast metrics for cross-polarization versus validated ship length.

4.3 RCS and contrast metrics versus incidence angle

We now consider the extracted RCS and contrast metrics as a function of the local incidence angle. The metrics for each polarization are shown in Figure 22 through Figure 25. The data gap around 37° incidence angle is due to IS5 mode not being available at the time of the data acquisition campaign. Again, linear fits to the data are included in each case so that the general trend is apparent.

Considering the segmented region contrast (the lower-right plot in each case), the target contrast is seen to improve with increasing incidence angle for co-polarization. This reflects the fact that the co-polarization clutter decreases with incidence angle, which drives recommendations to use larger incidence angles for ship detection. On the other hand, the target contrast is essentially independent of incidence angle for cross-polarization. This is due to the clutter being noise floor limited for cross-polarization. Recall that the noise floor is essentially independent of incidence angle.

The data filtering algorithm rejects low contrast (i.e., < 5 dB peak-to-clutter ratio) targets, which is evident as a lower limit in the contrast measures. Therefore, the best fit straight line that is plotted to show the general dependence on incidence angle has a slope that is biased low.

The segmented region RCS-to-clutter ratio as a function of incidence angle is shown in Figure 26 for both co-polarization (on the left) and cross-polarization (on the right). The data have been broken down by ship length population with the total population at the top, then the 1/3 smallest ships ($L \leq 100$ m), the middle 1/3 ships (100 m $< L \leq 160$ m), and the 1/3 largest ships ($L > 160$ m). The straight line fits, which are summarized in Figure 27, show how the observed contrast depends on the incidence angle, ship length, and polarization (for co-polarization and cross-polarization, at least). These plots illustrate how ships are more detectable for co-polarization data at larger incidence angles, and are more detectable for cross-polarization data at smaller incidence angles. The break-point between cross-polarization and co-polarization providing the best contrast depends on the ship length, but is seen to be around 33° (i.e., it is best to use cross-polarization for incidence angles smaller than 33°). This dependence on incidence angle reflects the decreasing clutter with increasing incidence angle for co-polarization, the noise floor limited clutter for cross-polarization, and the fact that the cross-polarization ship target RCS is about 10 dB smaller than the co-polarization ship target RCS.

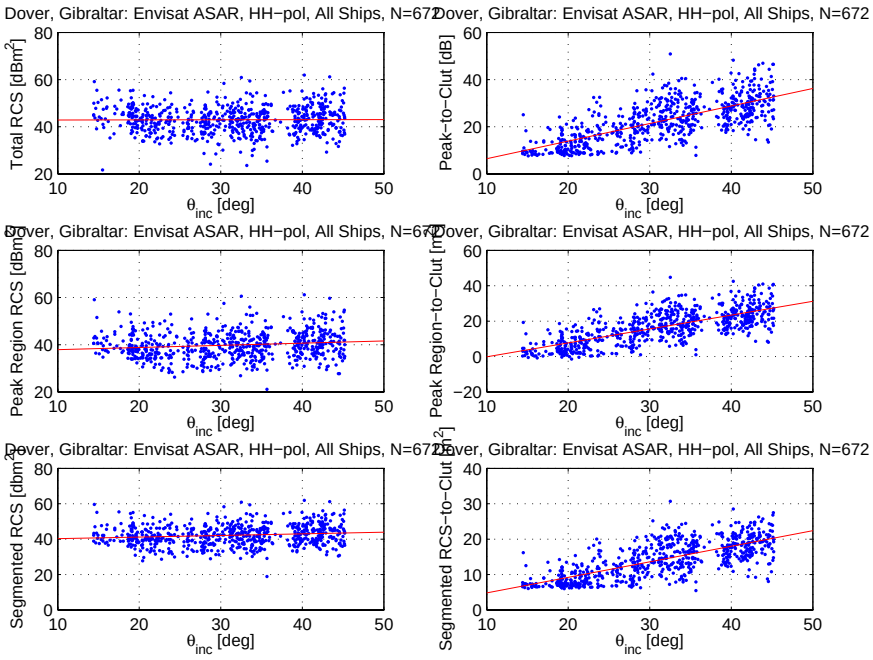

Figure 22: RCS and contrast metrics as a function of incidence angle for HH polarization.

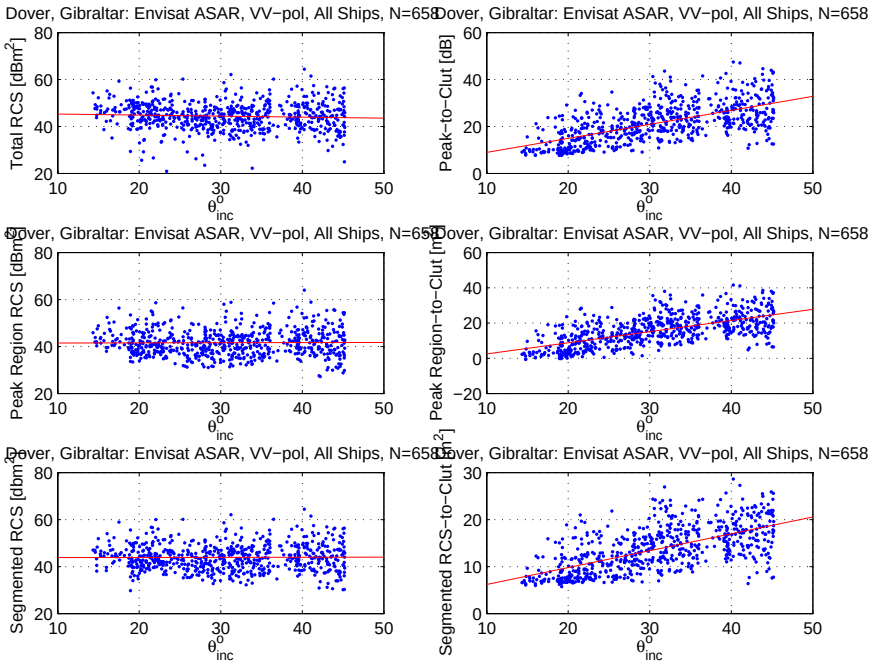

Figure 23: RCS and contrast metrics as a function of incidence angle for VV polarization.

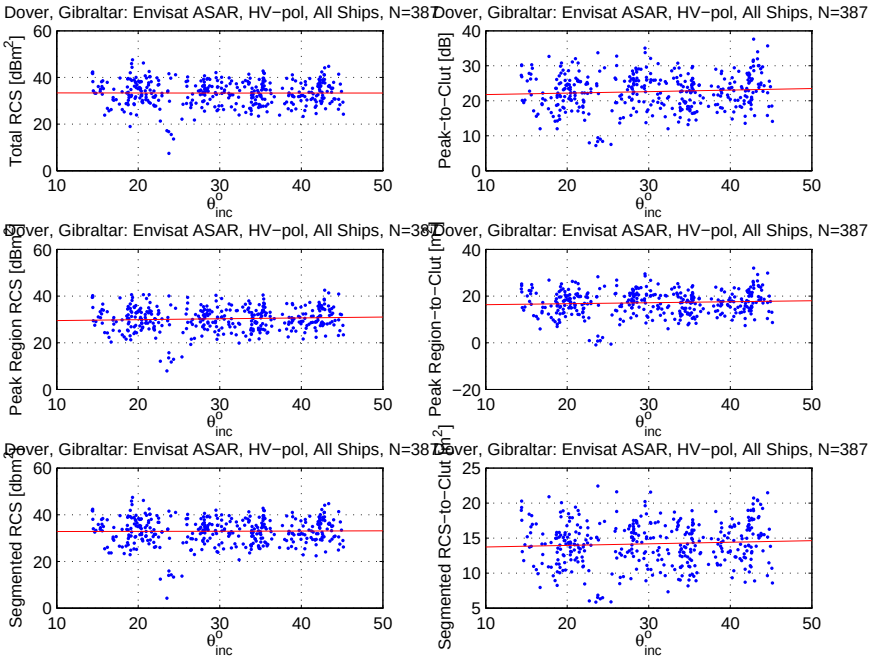

Figure 24: RCS and contrast metrics as a function of incidence angle for HV polarization.

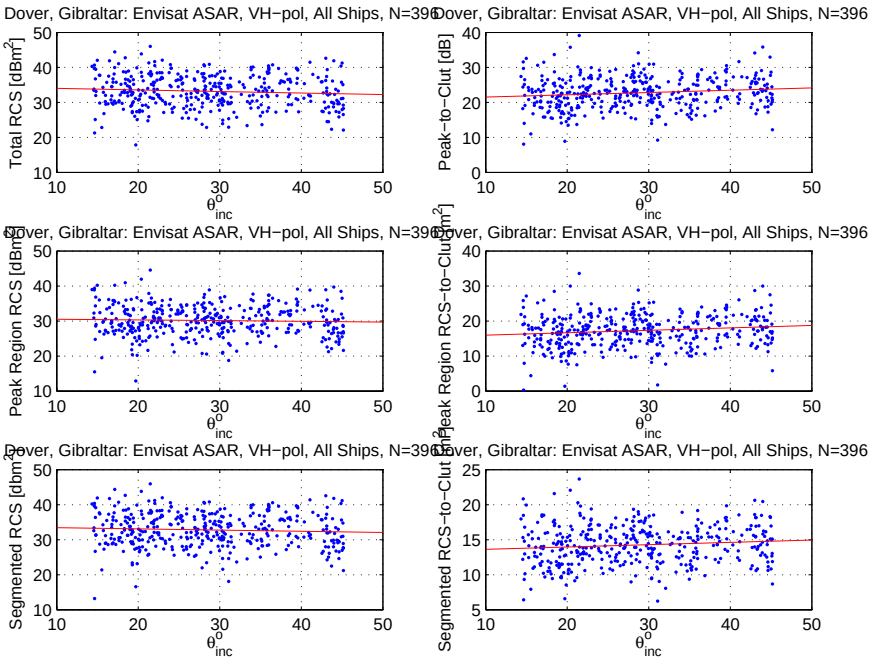

Figure 25: RCS and contrast metrics as a function of incidence angle for VH polarization.

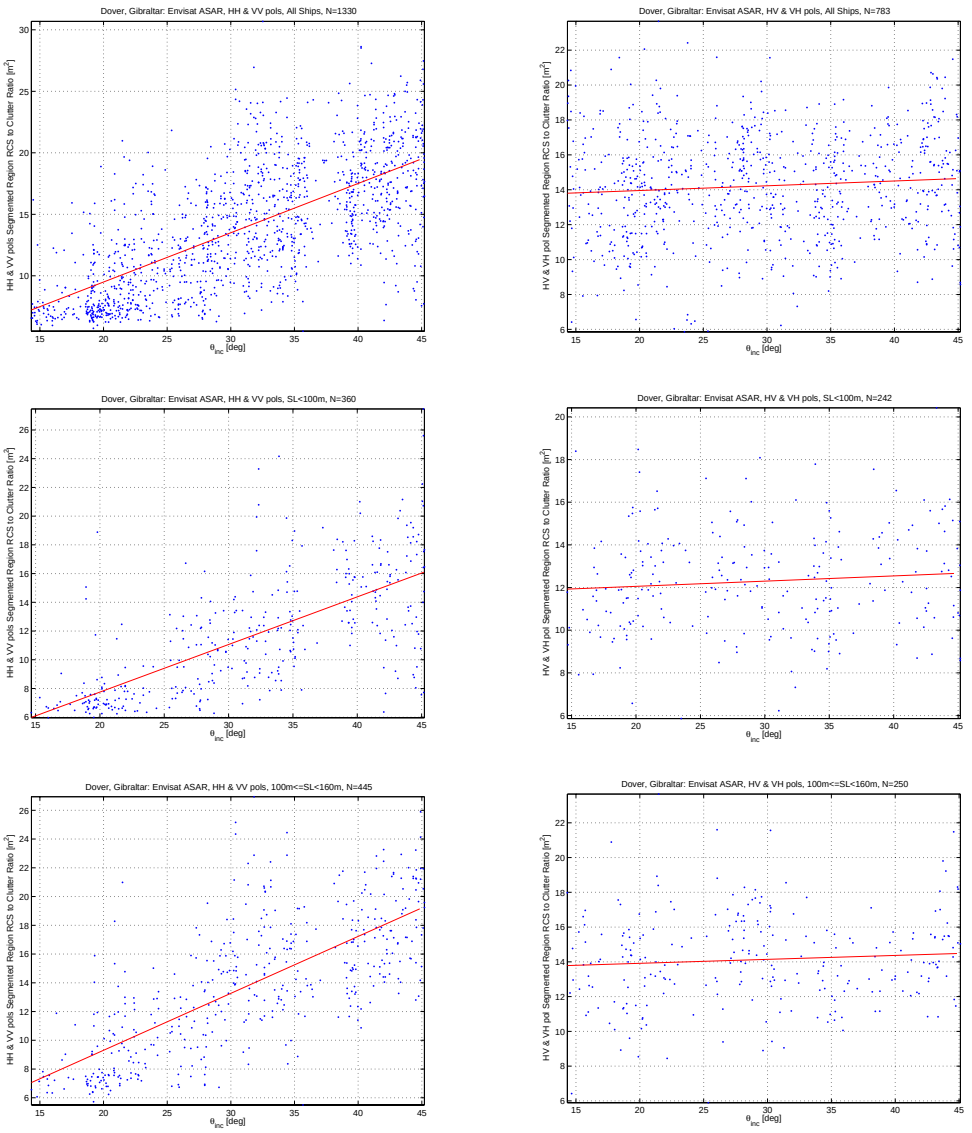

Figure 26: Segmented region RCS-to-clutter ratio for co-polarization (left) and cross-polarization (right) as a function of incidence angle for (top-to-bottom) all ships, smallest ships, medium ships, and longest ships. (Continued on next page.)

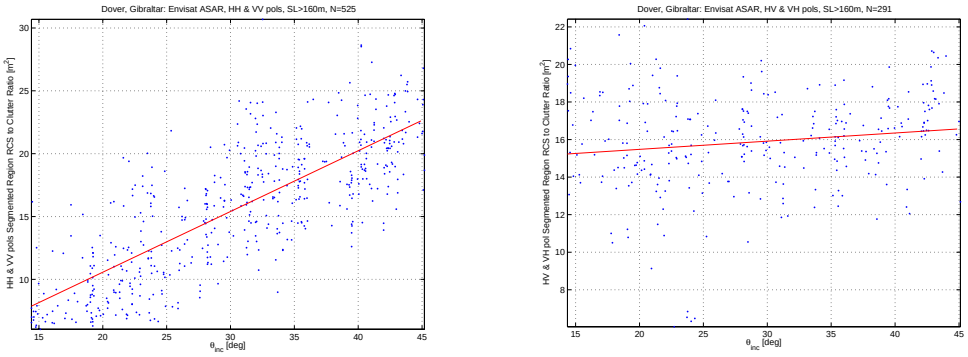

Figure 26: Concluded.

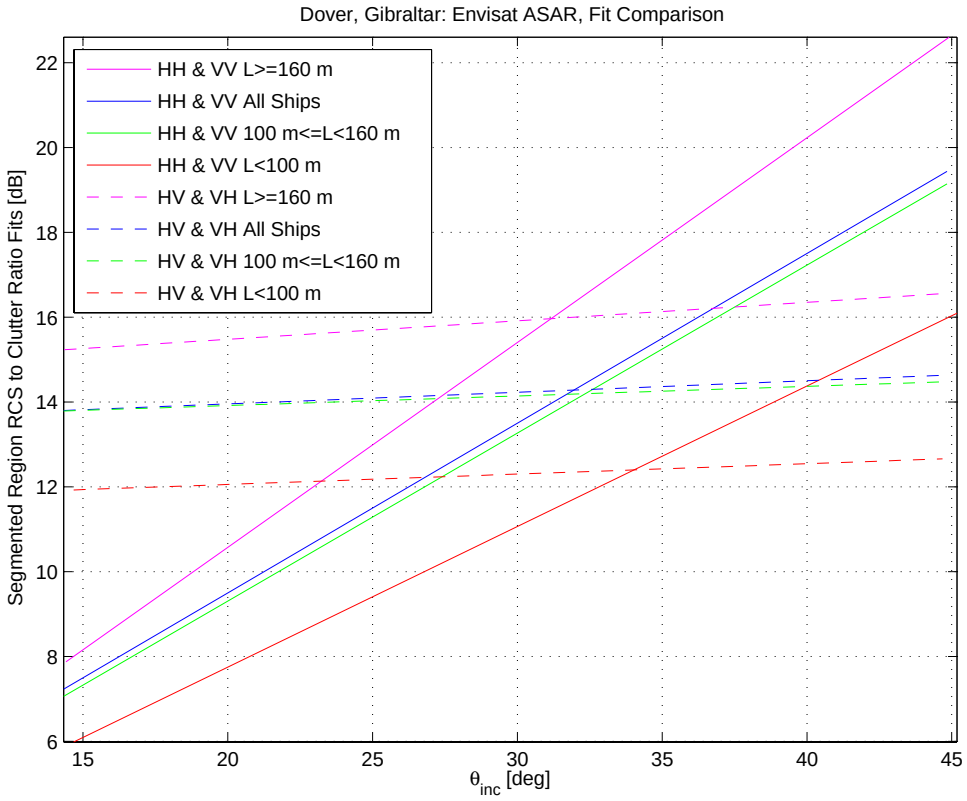

Figure 27: Summary of contrast as a function of incidence angle and ship length for both co-polarization and cross-polarization.

4.4 AP mode comparisons

Figure 28 shows scatterplots of total RCS measurements for each ship in the available AP modes. There are three such plots since there are three different AP modes available (i.e., HH/VV, HH/HV, and VV/VH).

From the plots, we see that the HH/VV total RCS values are well correlated. However, the co-polarization/cross-polarization Total RCS values do not appear to be as well correlated. Once again, the cross-polarization total RCS is about 10 dB smaller than the co-polarization total RCS.

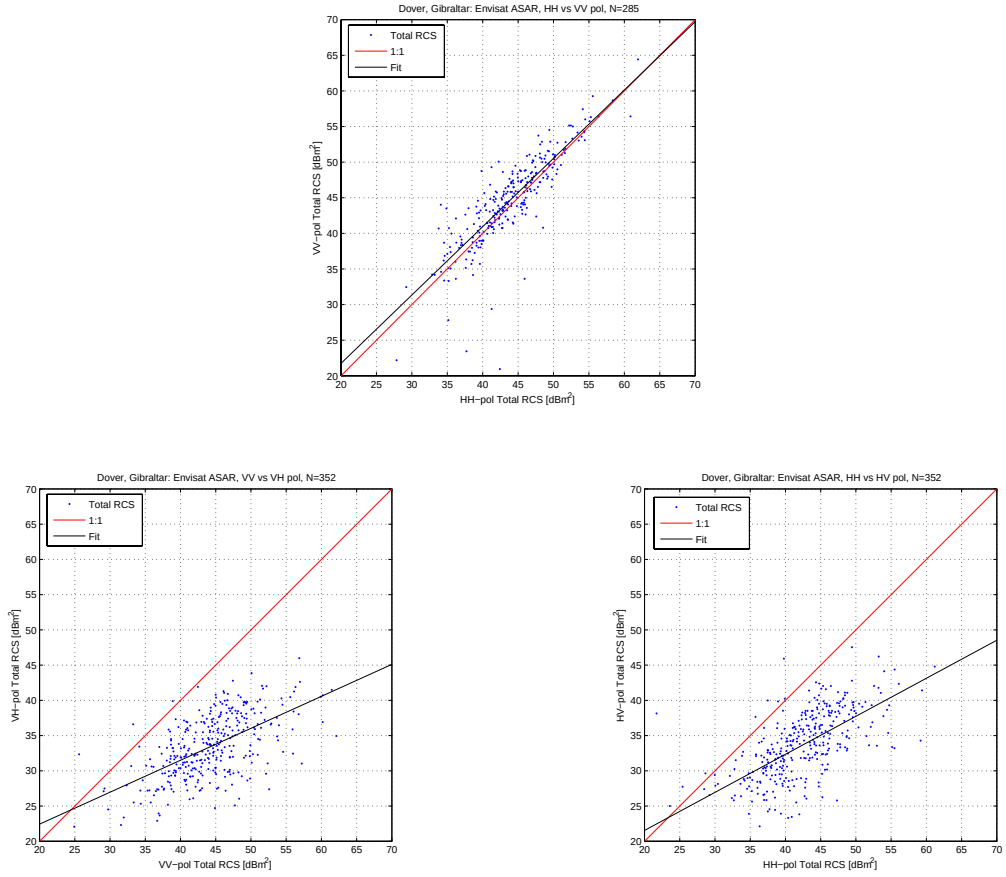

Figure 28: Scatterplots of total RCS for each AP mode.

5 PDF fits to the normalized total RCS

For each linear polarization, we tested various Probability Density Function (PDF) models to determine if they can describe the observed variability in the normalized total RCS distribution including Lognormal, Gamma, Weibull, Rayleigh, Ricean and Chi-Squared [1]. The normalization was carried out by dividing the observed total RCS value by the appropriate fitted total RCS of Table 3. The Kolomogorov-Smirnov (K-S) goodness-of-fit test was used to determine if the proposed PDF describes the observed variability (i.e., passes or fails).

From Table 3, we see that the Lognormal PDF describes the normalized RCS variability for both HH and VV polarizations, whereas the Gamma and Weibull PDFs are appropriate for HV polarization, and Lognormal and Gamma PDFs are appropriate for VH polarization. Figure 29 provides both the PDF and the corresponding Empirical Cumulative Density Function (ECDF) that passed the K-S test for each linear polarization. Figure 30 shows both the PDF and ECDF fits that passed the K-S test for the combined co-polarization and cross-polarization data sets. Table 4 summarizes the results and provides the model fit parameters[1] along with the 10% and 90% cumulative probability values for the fitted PDFs. The results indicate that the co-polarization data are less dispersed than the cross-polarization data. Furthermore, the provided PDFs could be used as inputs to ship detection software to guide the probability of missed detection, or could be used to improve ship detectability prediction for future SAR missions.

Table 4: Model fit results for each linear polarization and combined polarizations.

Pol	***Model Fit***	***A***	***B***	***10%***	***90%***
HH	Lognormal	5.7560e-15	1.0586	0.26	3.88
VV	Lognormal	–5.3544e-15	1.0758	0.25	3.97
HV	Gamma	1.7189	0.79979	0.32	2.78
HV	Weibull	1.4999	1.3352	0.39	4.16
VH	Lognormal	2.7560e-15	0.70430	0.41	2.47
VH	Gamma	2.1870	0.58462	0.37	2.44
Co-Pol	Lognormal[2]	–6.1020e-3	1.0661	0.25	3.89
Cross-Pol	Gamma	1.9049	0.69799	0.34	2.62

[1] In Table 4 and the subsequent plots, the *A* and *B* parameters correspond respectively to the Shape and Scale parameters for the Gamma distribution, the Scale and Shape parameters for the Weibull distribtuion, and *mu* and *sigma* for the Lognormal distribution. The PDFs are as defined in Matlab®.

[2] The two largest normalized total RCS values were filtered from the dataset in order for the model to pass the K-S test.

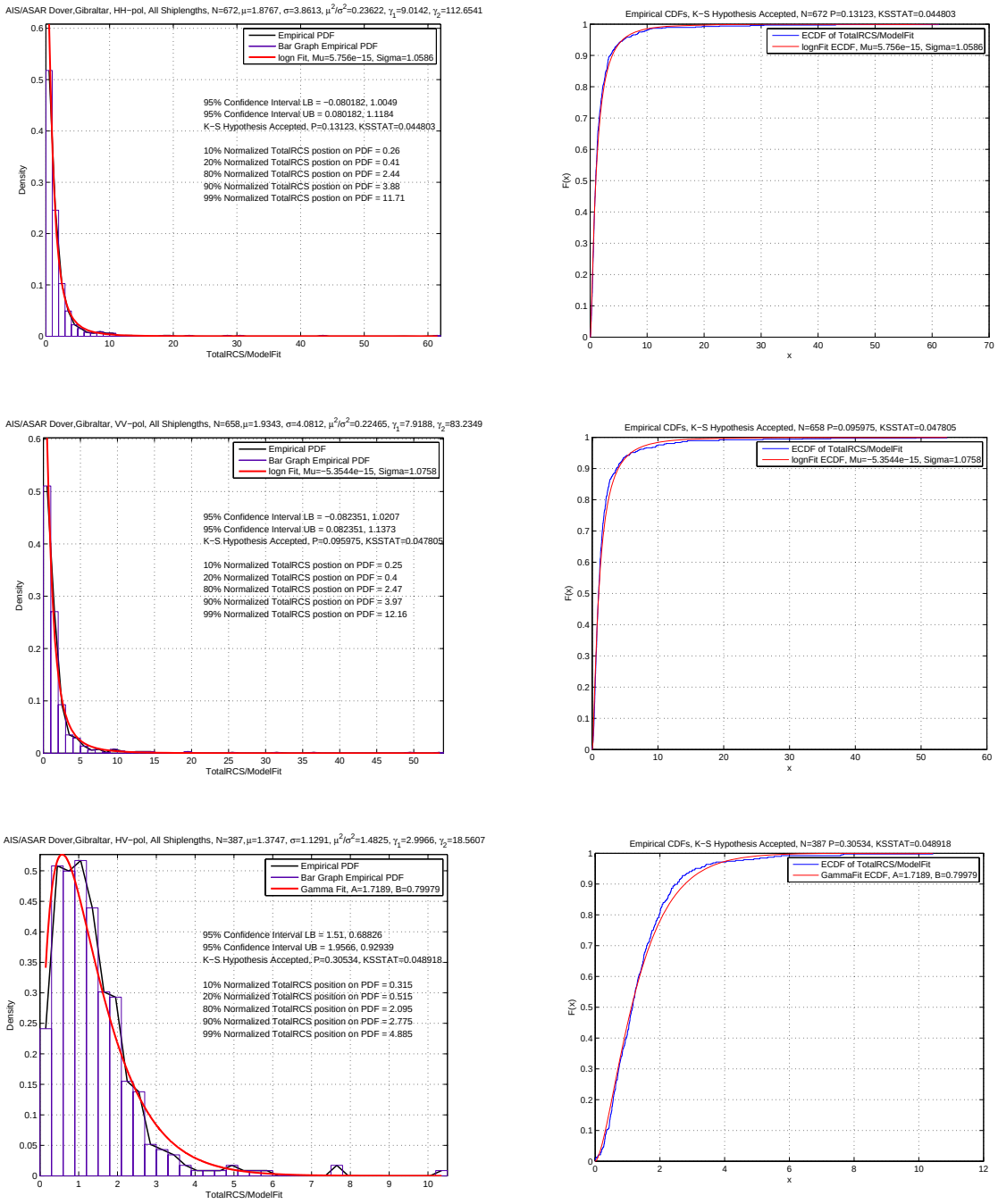

Figure 29: PDF (left) and ECDF (right) for each linear polarization that passed the K-S goodness-of-fit test. (Continued on next page.)

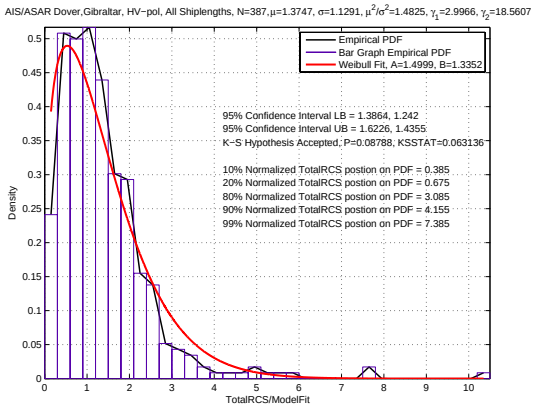

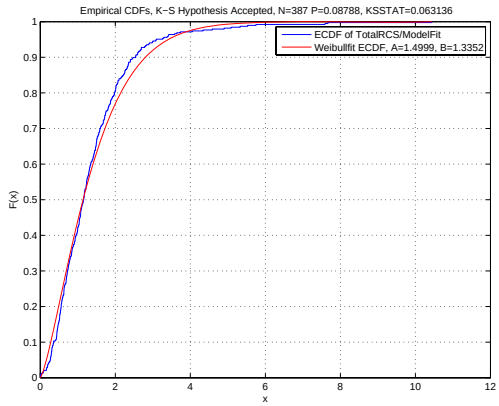

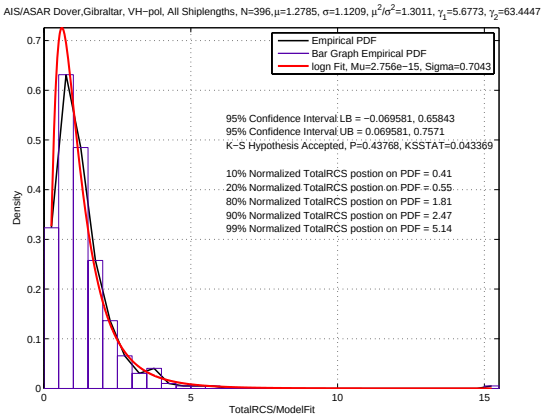

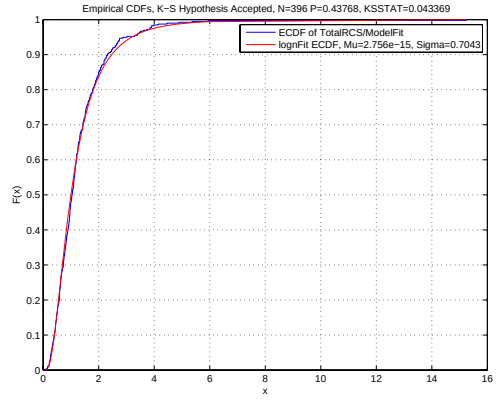

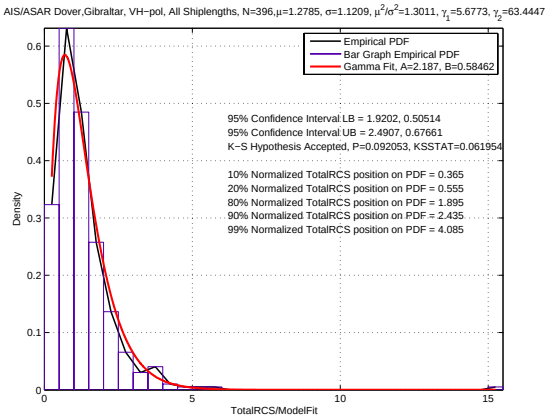

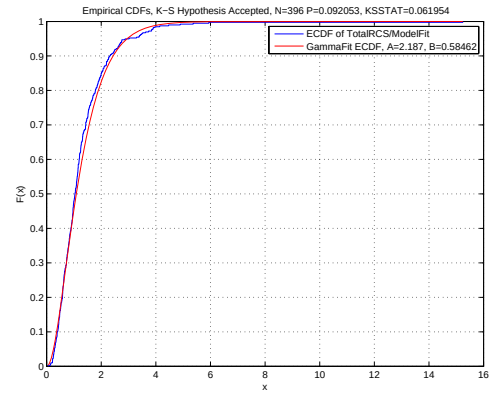

Figure 29: Concluded.

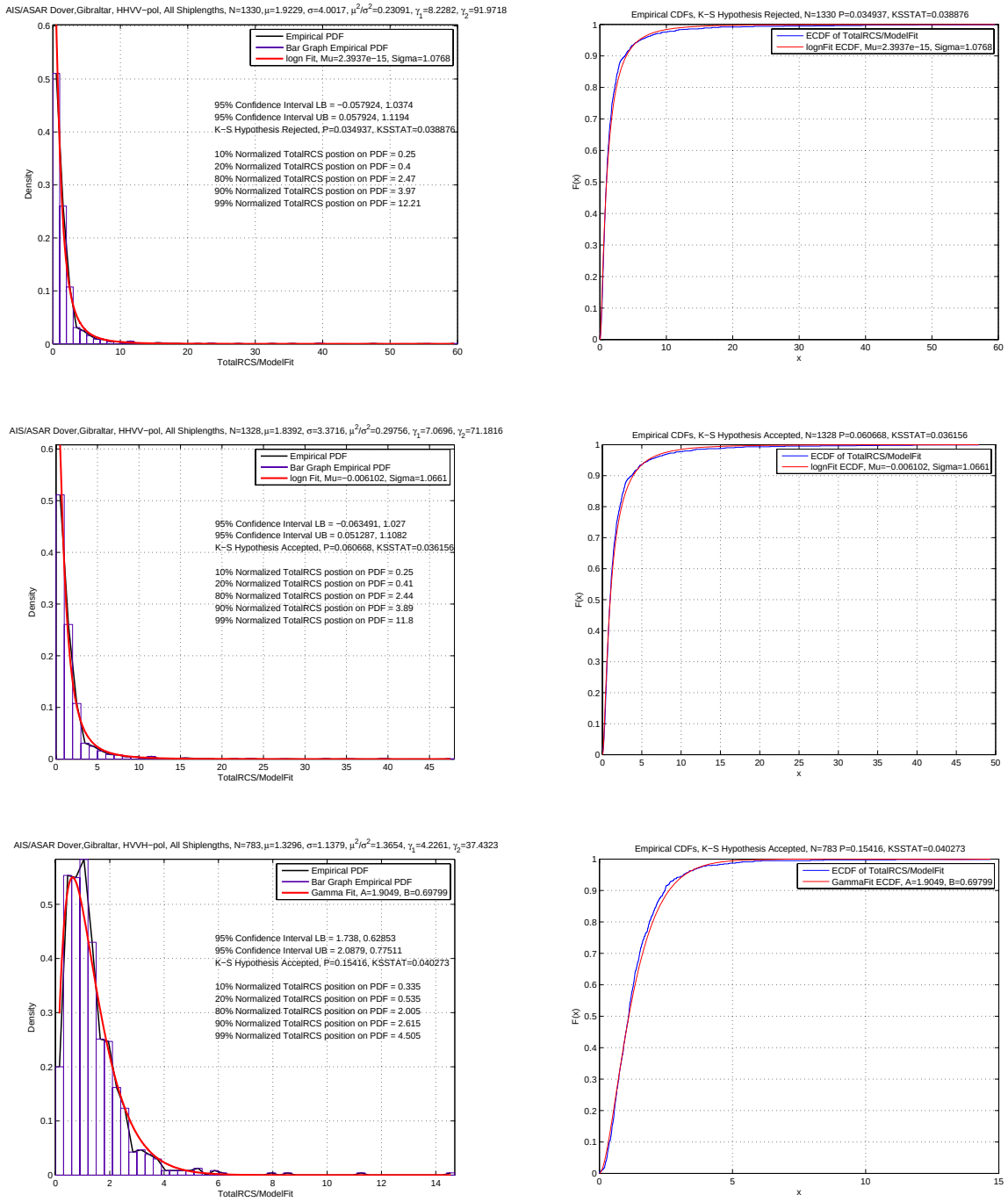

Figure 30: Combined co-polarization and cross-polarization PDF (left) and ECDF (right). The original co-polarization data set (1st row) did not pass the K-S test; however, it does pass the K-S test (2nd row) after removing the two largest normalized total RCS samples from the data set.

6 Target signature length estimates

Although there are many approaches to ship signature length estimation, in this work we have focussed on the results from VUSAR [8], a tool that is in routine use at DRDC Ottawa and has been extended for ship signature analysis. VUSAR segments the ship signature from the background clutter by using a thresholding operation, followed by a sequence of morphological operations to better define the signature's shape. Derived ship length estimates are expected to be representative of results from other ship signature analysis tools. Figure 31 shows scatterplots of ISR database validated ship length and the VUSAR-measured ship length estimates for each linear polarization. We note that there is fairly good correlation for all polarizations, but that there are occurrences of ship length under and over estimation. The occurrences of these conditions will be considered in greater detail.

Figure 32 provides histograms of the error measurement $\varepsilon = \Delta L/L$ where ΔL = (VUSAR measured ship signature length – ISR database validated ship length) and L is the ISR database validated ship length. The red vertical lines to the left and right of zero in each plot represent the 30% error tolerance locations that were considered previously. The rates of occurrence are summarized in Table 5. The "$\varepsilon < -0.3$" column represents the percentage of ship length estimates below the 30% error tolerance, while the "$\varepsilon > 0.3$" represents the percentage of ship length estimates above the 30% error tolerance. For co-polarization we see a considerably larger rate of underestimation of ship length (approximately 27%) than for cross-polarization (approximately 6%). Presumably this arises since the clutter levels are higher, often masking part of the ship signature. On the other hand, for cross-polarization we see a considerably larger rate of overestimation of ship length (approximately 22%) than for co-polarization (approximately 12%). This result is somewhat surprising since we expect that the degree of azimuth signature smearing due to ship motion should be independent of polarization. However, it is possible that the generally high contrast ratio for cross-polarization might more clearly show signature sidelobes or other imaging artefacts that are being measured as part of the ship length.

Table 5: Breakdown of all ship length estimates.

	All Ships		
Pol	**N**	**$\varepsilon < -0.3$ [%]**	**$\varepsilon > 0.3$ [%]**
HH	654	26.8	13.3
VV	633	28.9	10.9
HV	373	6.7	23.6
VH	392	6.1	20.7

In the balance of this section, we investigate dependencies of target signature length estimates on incidence angle, target-to-clutter ratio, and ship aspect angle.

Figure 33 shows scatterplots of ISR database validated ship length and the VUSAR measured ship length for each linear polarization. The red points represent ships with $\theta_{inc} < 25°$ and the blue points represent ships with $\theta_{inc} \geq 25°$. For co-polarization, there are more underestimates of ship length at lower incidence angles, as observed by the large number of red points that appear below the 1:1 fit line. For cross-polarization, there are very few underestimates observed at all

incidence angles. There are more overestimates of ship length for cross-polarization. Figure 34 provides the ΔL/L histogram for ships with $\theta_{inc} < 25°$, while Figure 35 provides the ΔL/L histogram for ships with $\theta_{inc} \geq 25°$. Table 6 summarizes the results.

Table 6: Breakdown of ship length estimates by incidence angle.

	All Ships			**$\theta_{inc} < 25°$**			**$\theta_{inc} \geq 25°$**		
Pol	**N**	**ε < –0.3 [%]**	**ε > 0.3 [%]**	**N**	**ε <– 0.3 [%]**	**ε > 0.3 [%]**	**N**	**ε < –0.3 [%]**	**ε > 0.3 [%]**
HH	654	26.8	13.3	171	64.9	5.8	483	13.2	17.0
VV	633	28.9	10.9	174	64.4	4.0	459	14.8	13.7
HV	373	6.7	23.6	117	9.4	30.8	256	5.9	20.3
VH	392	6.1	20.7	154	7.1	23.4	238	5.4	23.3

Figure 36 shows scatterplots of ISR database validated ship length and the VUSAR measured ship length for each linear polarization. In this case, the red points represent ships with TCR[3] < 10 dB and the blue points represent ships with TCR ≥ 10 dB. For co-polarization, a significant number of ships are underestimated at low TCRs, as observed by the large number of red samples that fall below the 1:1 fit line. For cross-polarization, there are very few underestimates observed. There appears to be more overestimates of ship length for cross-polarization. Figure 37 provides the ΔL/L histogram for ships with TCR < 10 dB, while Figure 38 provides the ΔL/L histogram for ships with TCR ≥ 10 dB. Table 7 summarizes the results.

Table 7: Breakdown of ship length estimates by TCR.

	All Ships			**TCR < 10 dB**			**TCR ≥ 10 dB**		
Pol	**N**	**ε < –0.3 [%]**	**ε > 0.3 [%]**	**N**	**ε < –0.3 [%]**	**ε > 0.3 [%]**	**N**	**ε < –0.3 [%]**	**ε > 0.3 [%]**
HH	654	26.8	13.3	175	63.4	9.1	479	13.8	16.3
VV	633	28.9	10.9	157	66.9	9.6	476	16.2	10.5
HV	373	6.7	23.6	29	17.2	41.4	344	5.8	22.1
VH	392	6.1	20.7	21	28.6	33.3	371	4.9	20.2

Figure 39 shows scatterplots of ISR database validated ship length and the VUSAR measured ship length for each linear polarization. In this case, the red points represent azimuth travelling ships (i.e., within ±45° of travelling along the azimuth direction, parallel or anti-parallel to the satellite track) and the blue points represent range travelling ships (i.e., within ±45° of travelling along the range direction, towards or away from the satellite). For both co-polarization and cross-polarization, most of the larger overestimates are azimuth travelling ships. Figure 40 provides the ΔL/L histogram for range travelling ships and Figure 41 provides the ΔL/L histogram for azimuth travelling ships. Table 8 summarizes the results.

[3] Represented by the segmented region RCS-to-clutter ratio.

Table 8: Breakdown of ship length estimates by ship aspect angle.

	All Ships			Range Travelling			Azimuth Travelling		
Pol	**N**	**ε < –0.3 [%]**	**ε > 0.3 [%]**	**N**	**ε < –0.3 [%]**	**ε > 0.3 [%]**	**N**	**ε < –0.3 [%]**	**ε > 0.3 [%]**
HH	654	26.8	13.3	444	22.8	9.9	210	33.3	20.5
VV	633	28.9	10.9	487	27.7	8.8	146	32.2	15.1
HV	373	6.7	23.6	234	7.7	10.3	139	4.3	48.9
VH	392	6.1	20.7	318	6.6	14.8	74	4.1	51.4

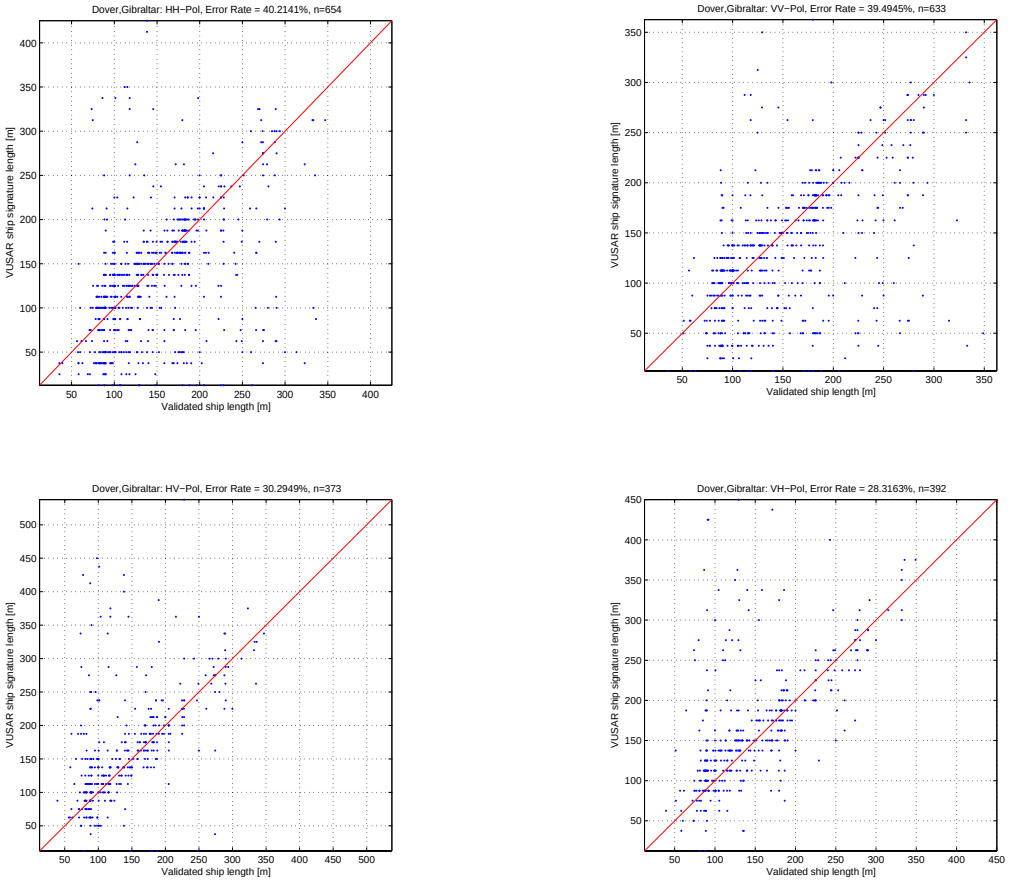

Figure 31: Scatterplots of VUSAR ship length and ISR Database validated ship length for each linear polarization.

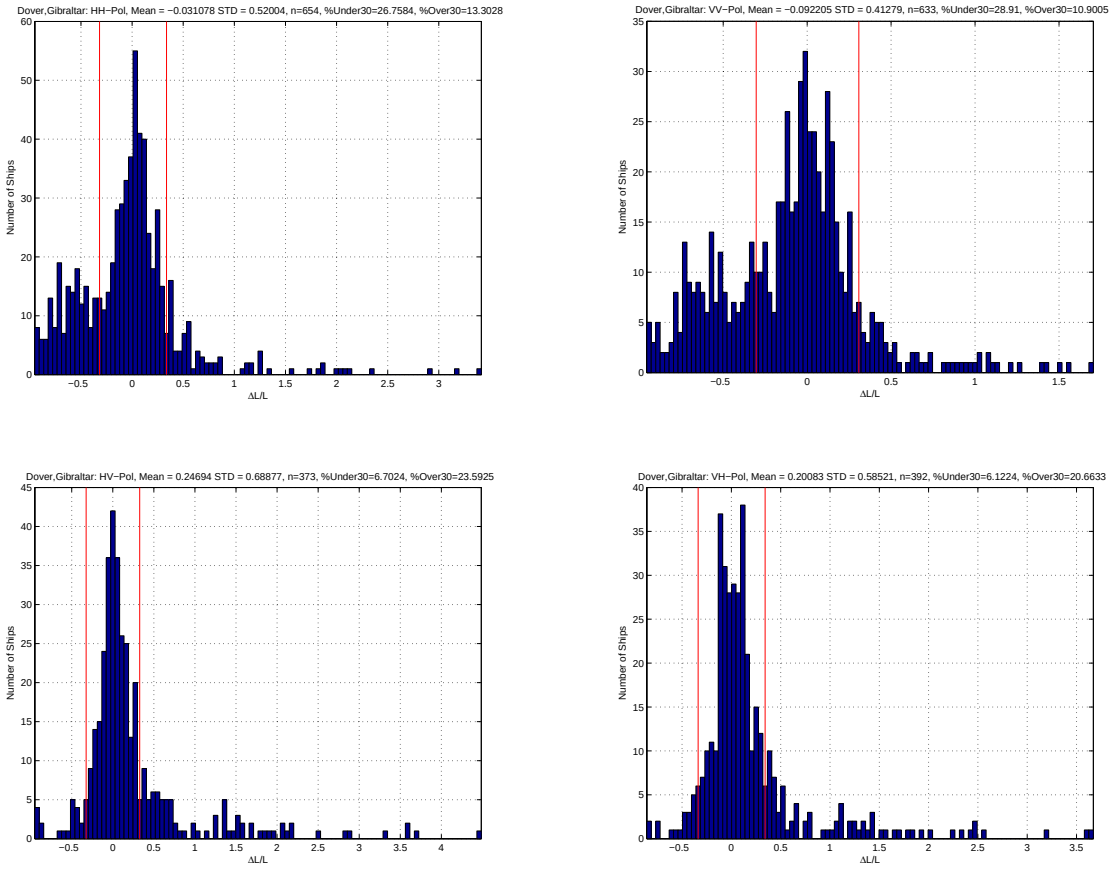

Figure 32: Histograms of ΔL/L showing the 30% error positions (red lines) for each linear polarization.

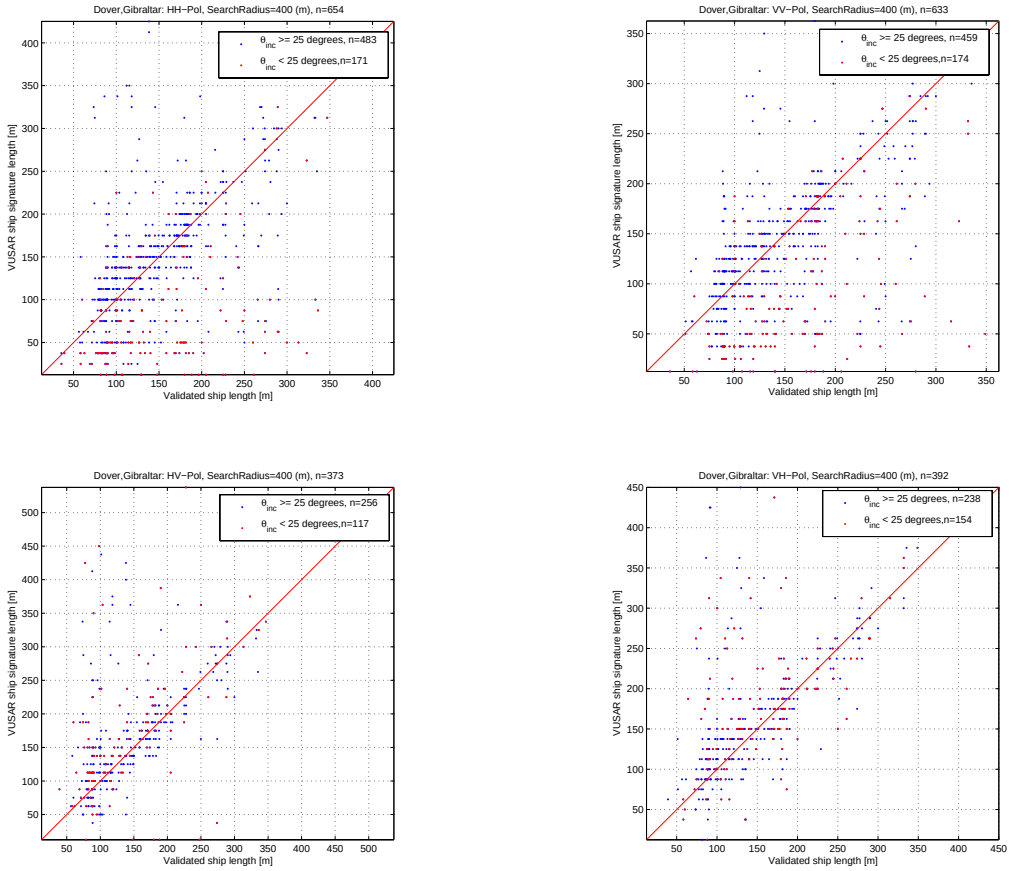

Figure 33: Scatterplots of VUSAR ship length and ISR Database validated ship length for each linear polarization. The blue points indicate ships at incidence angles ≥ 25° while the red points indicate ships at incidence angles < 25°.

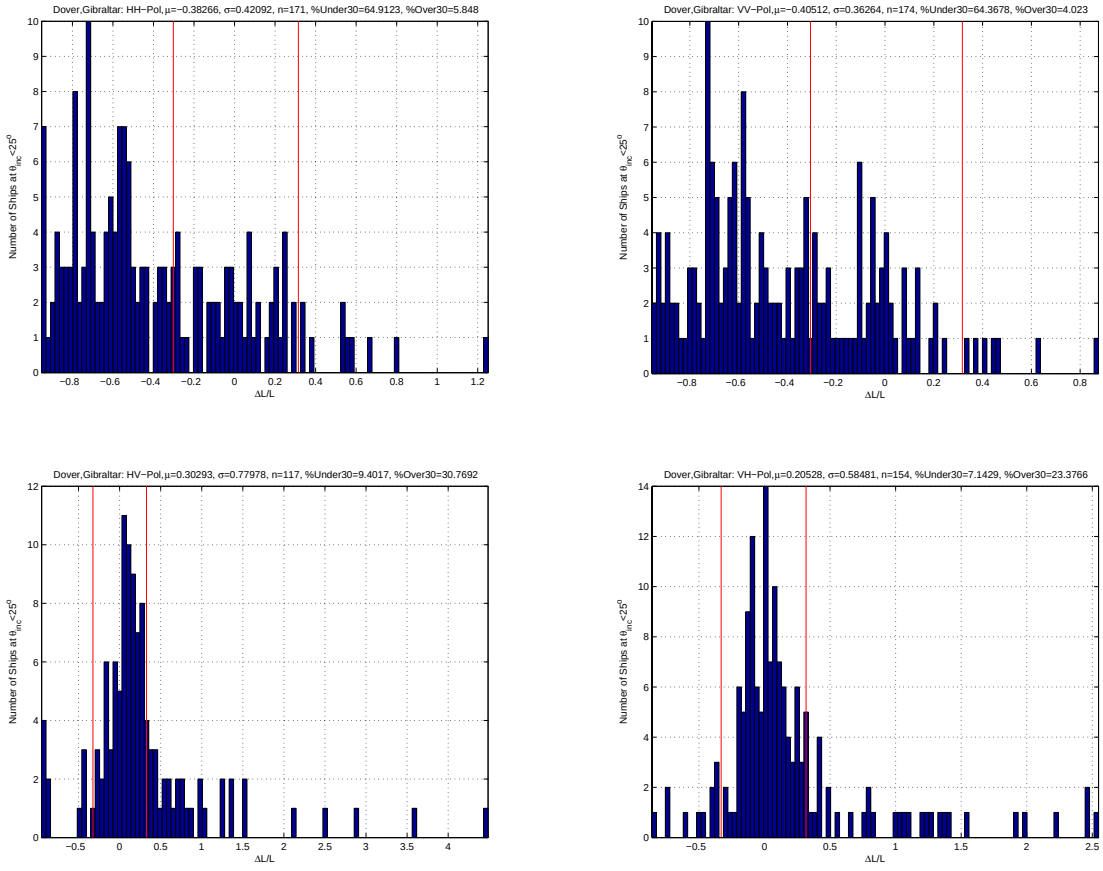

Figure 34: Histograms of ΔL/L for ships at incidence angles < 25° showing the 30% error positions (red lines) for each linear polarization.

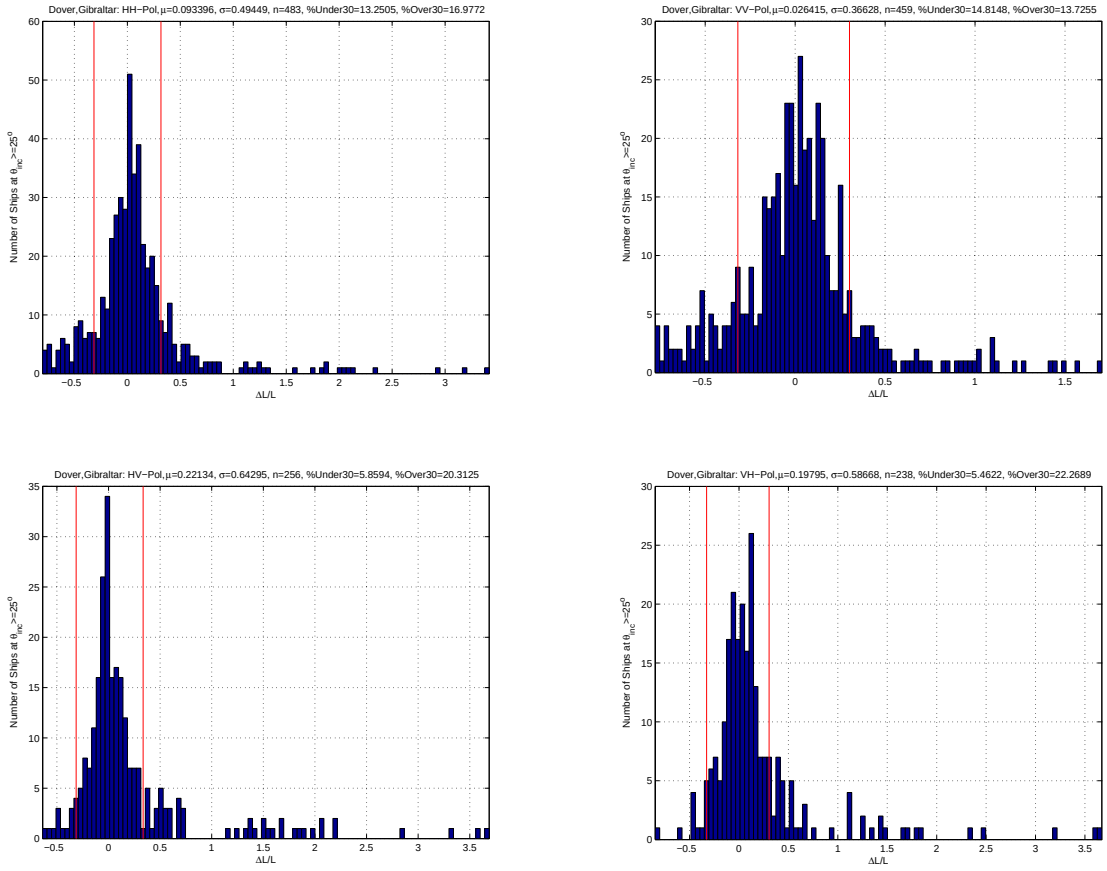

Figure 35 Histograms of ΔL/L for ships at incidence angles ≥ 25° showing the 30% error positions (red lines) for each linear polarization.

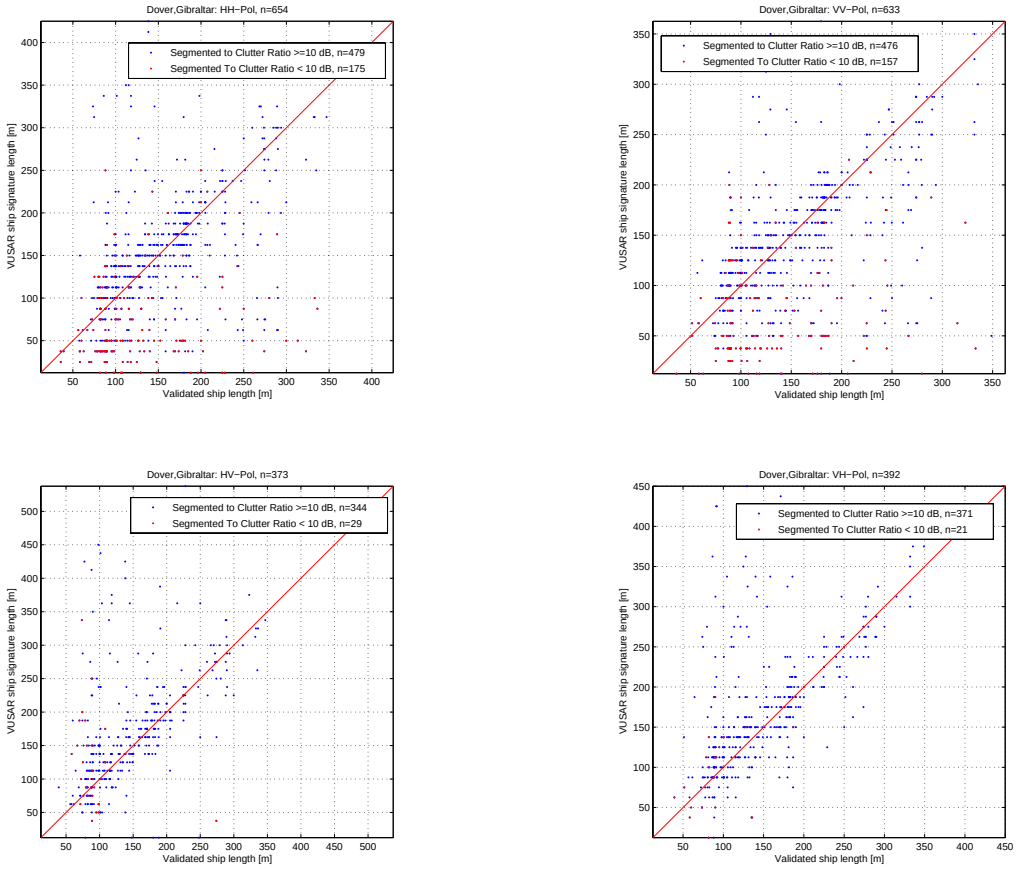

Figure 36: Scatterplots of VUSAR ship length and ISR Database validated ship length for each linear polarization. The blue points indicate ships with TCR ≥ 10 dB while the red points indicate ships with TCR < 10 dB.

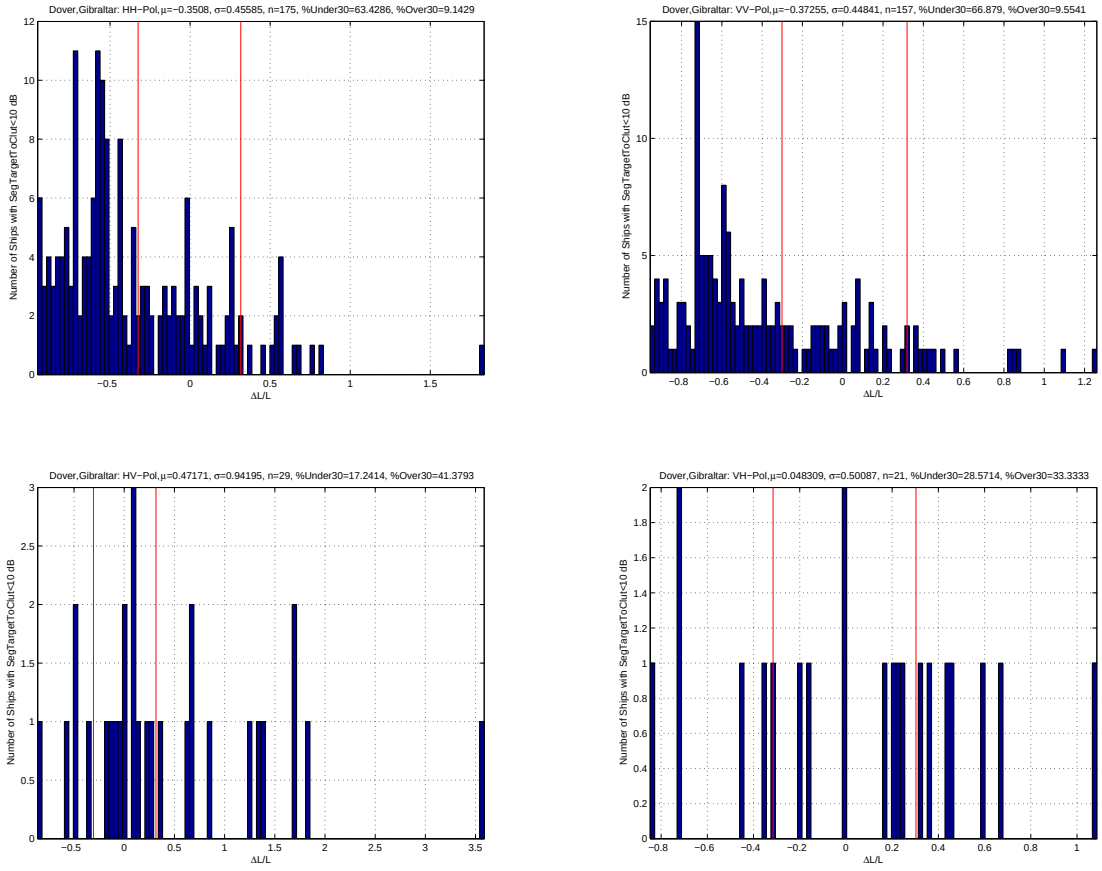

Figure 37: Histograms of ΔL/L for ships with TCR < 10 dB showing the 30% error positions (red lines) for each linear polarization.

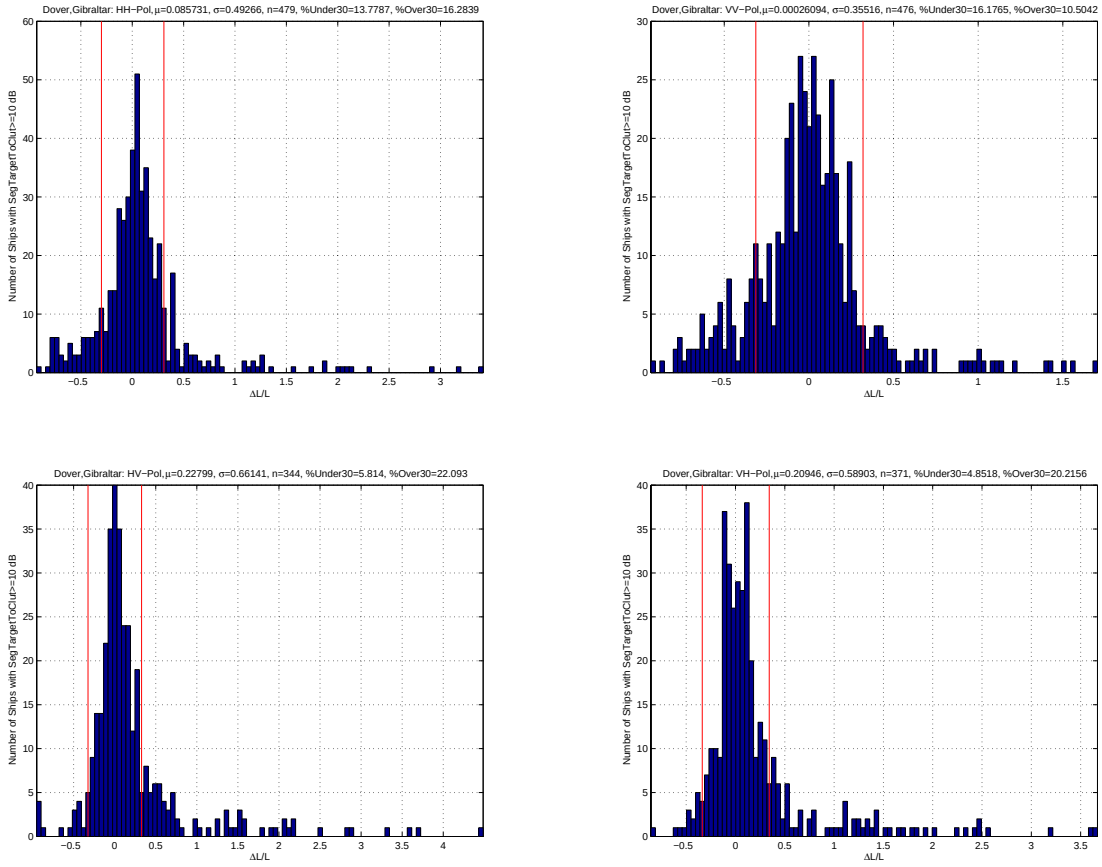

Figure 38: Histograms of ΔL/L for ships with TCR ≥ 10 dB showing the 30% error positions (red lines) for each linear polarization.

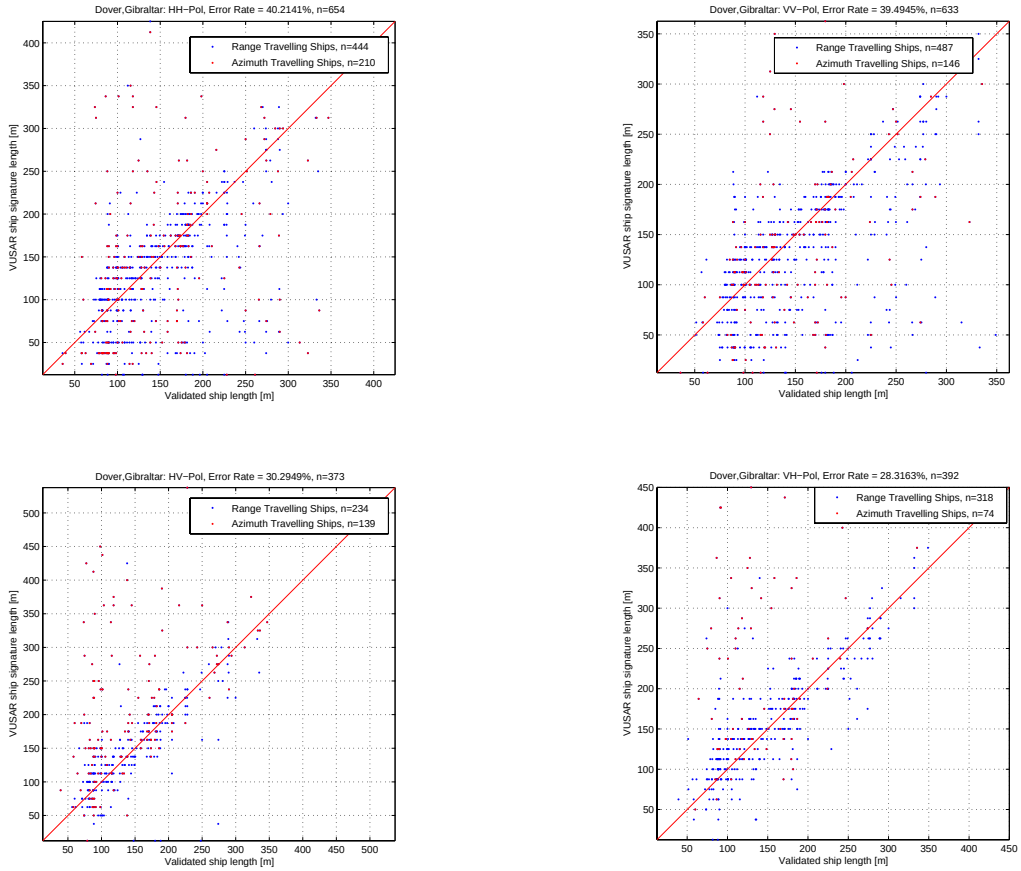

Figure 39: Scatterplots of VUSAR ship length and ISR Database validated ship length for each linear polarization. The blue points indicate range travelling ships while the red points indicate azimuth travelling ships.

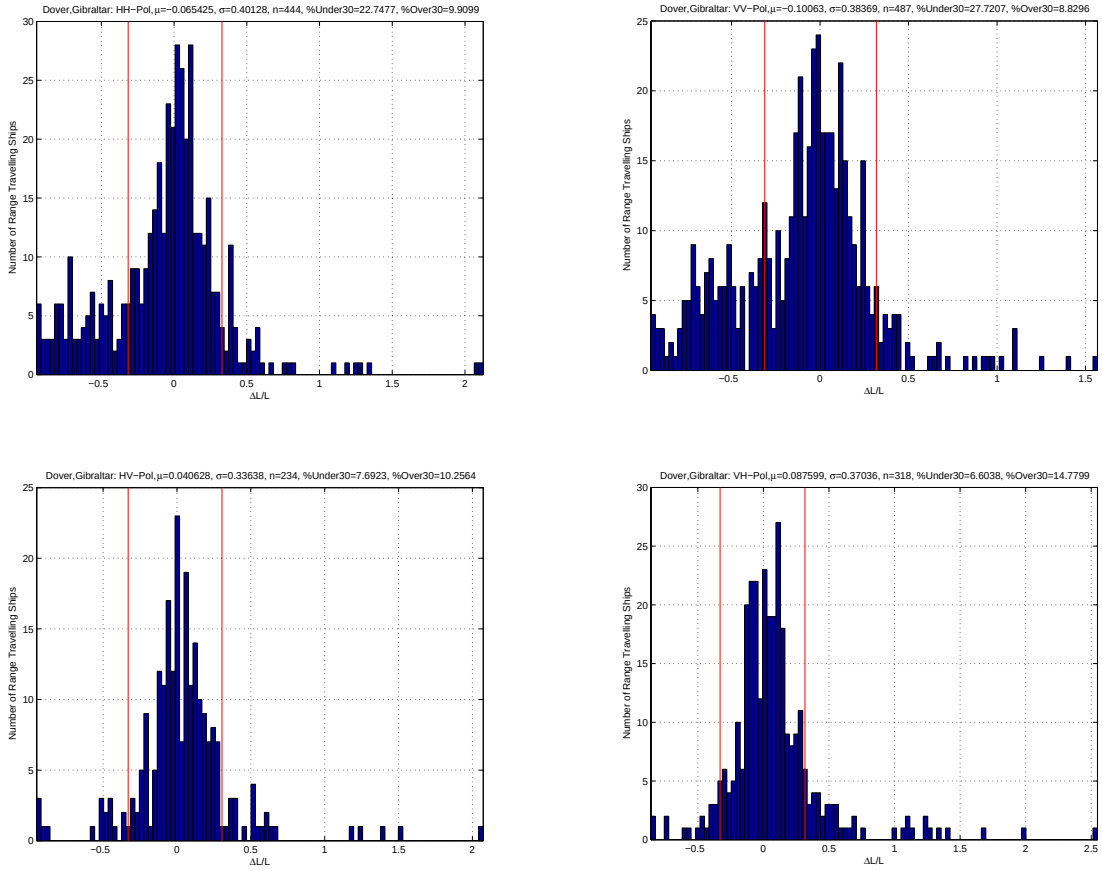

Figure 40: Histograms of ΔL/L for range travelling ships showing the 30% error positions (red lines) for each linear polarization.

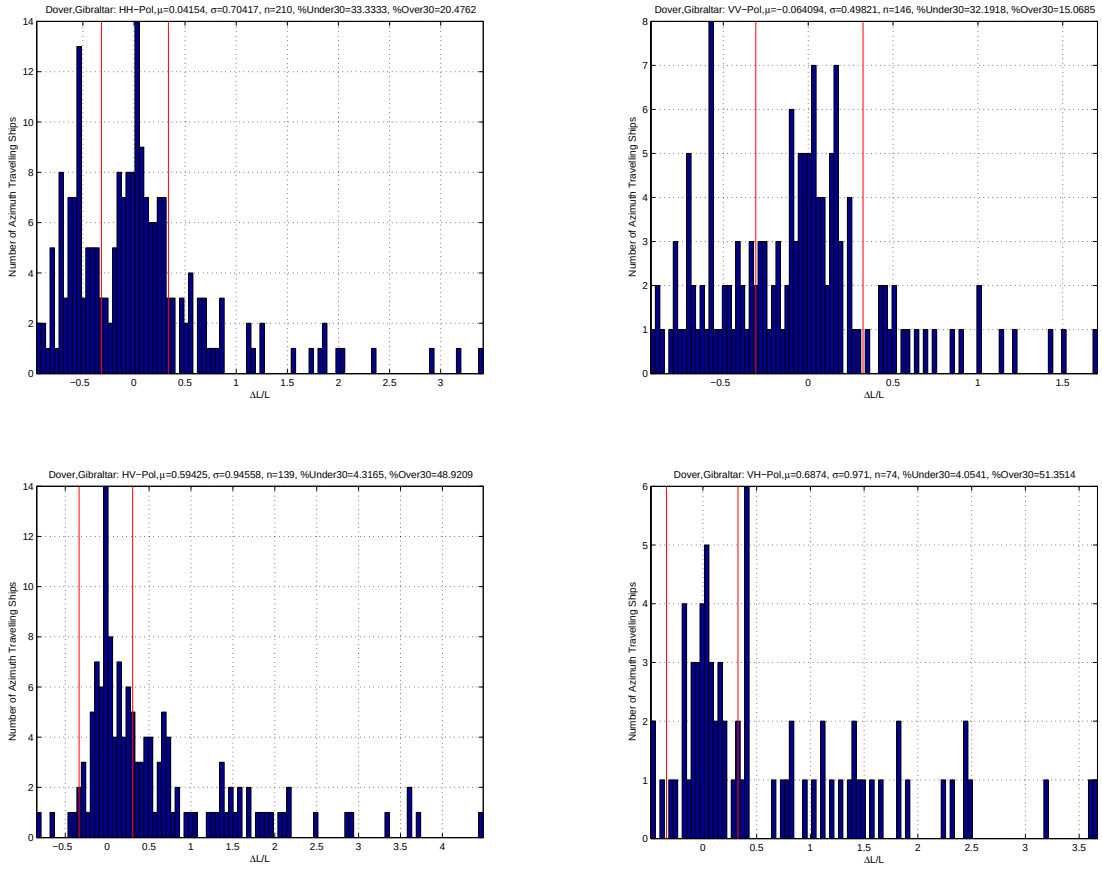

Figure 41: Histograms of ΔL/L for azimuth travelling ships showing the 30% error positions (red lines) for each linear polarization.

7 Ship wakes

It is well known that ship wakes appear in SAR ocean images, and that ship wakes are most visible under moderate wind conditions when the clutter-to-noise ratio is relatively high. A new observation from this data set is that there is a signature related to ship wakes in the cross-polarization data.

Figure 42 and Figure 43 show the nature of the observed ship wakes in both co-polarization and cross-polarization data. This IS3 image was acquired on 27 November 2006 with HH and HV channels. In the figures, the blue line is the projected ship track as calculated from the AIS data; the intersection of the blue and yellow lines represents the AIS-projected ship position; the opposite end of the yellow line at or near the ship target signature position represents the AIS-predicted ship position, which accounts for azimuth shifting due to the radial component of ship velocity. The blue lines lie along several wakes that appear as linear features in the HH data. The 'zooms' illustrate that the ship signature is deterministically shifted in azimuth with respect to the ship wake by an amount that is predicted by the length of the yellow line. Of particular interest is the ghost ship signature that is present for some ships in the HV data. The ghost signature is thought to be related to the ship wake since the signature is not subject to the azimuth shift associated with the radial component of the ship velocity. Due to low clutter levels, wakes are not expected to be visible in cross-polarized data. However, it is possible that the ghost signature could be related to scattering off the bow wave of the ship.

All of the Envisat ASAR images acquired were scanned for the occurrence of ship wake signatures in each available polarization channel. It was found that linear ship wake signatures were not visible in approximately 50% of the co-polarization images that were acquired. Of course, the co-polarization ship wakes were not necessarily visible for every ship in the image that included ship wakes. The co-polarization ship wakes were more visible for smaller incidence angles when the clutter (i.e., wind speed) wasn't too high. On the other hand, some cross-polarization wakes were visible in all of the images that were acquired. Again, the cross-polarization ship wakes were not necessarily visible for every ship in a particular image.

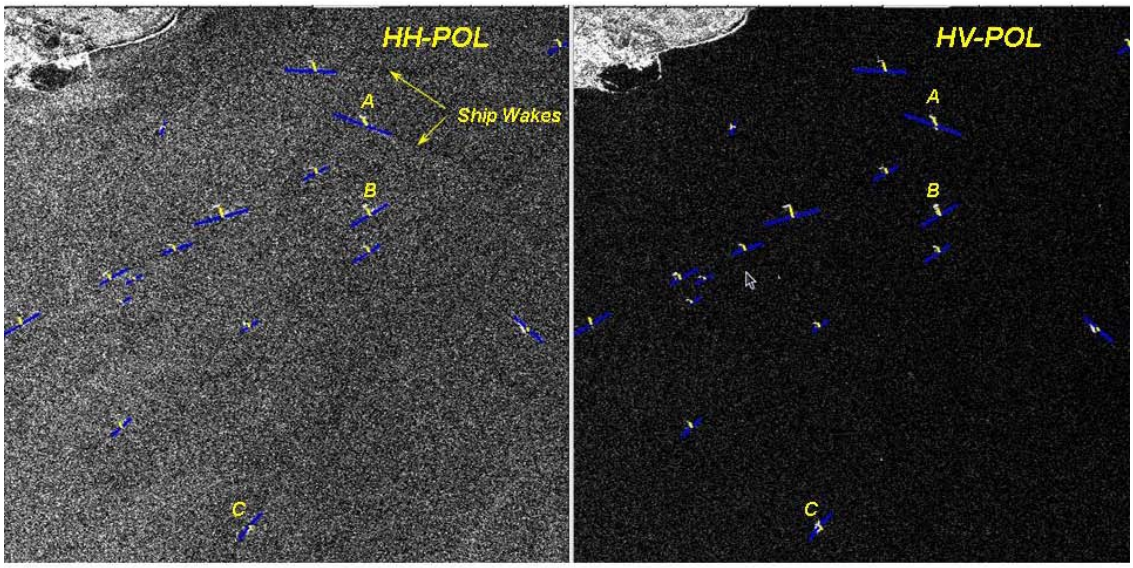

Figure 42: Ship wakes observed in the IS3 Dover image acquired on 27 November 2006.

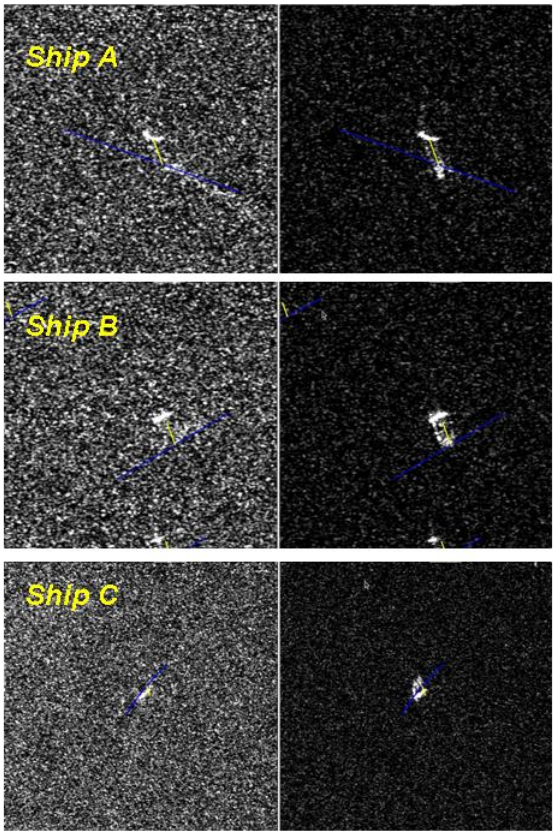

Figure 43: Zooms of ships A, B, and C of Figure 42 in both HH (left) and HV (right) polarizations.

8 Conclusions

We have successfully used AISLive data to validate ship signatures in Envisat ASAR AP mode imagery. The data sets were acquired over high density shipping in the Strait of Dover and the Strait of Gibraltar. This work extends previous studies that focussed on R-1 Fine and SCNB modes.

In total, 35 dual polarization images were acquired. These images included 672 validated ships for HH polarization, 658 for VV, 387 for HV, and 396 for VH. The AISLive validation data were verified through the ISR database, using the IMO number as a cross reference. The mean distance between the AIS-predicted ship position and the actual ship signature position was around 150 m, which is roughly the size of the average ship in the validation database.

This data set has provided new insight to ship detectability in SAR ocean imagery. For example, at co-polarization and for smaller incidence angles, ships may not be visible at all. On the other hand, the ship is usually clearly visible in the corresponding cross-polarization channel.

For each validated ship, several metrics were computed using the VUSAR tool. These included the clutter statistics, the total RCS of each ship, and the ship signature length. These metrics were evaluated in terms of the polarization, the local incidence angle, the validated ship length, the target-to-clutter ratio, and the ship aspect angle. The following is apparent:

- For co-polarization, the ocean clutter decreases with increasing incidence angle. For cross-polarization, the ocean clutter rarely exceeds the instrument noise floor. Therefore, the cross-polarization clutter is at the Envisat ASAR noise floor, so any contrast metrics would be relative to the instrument noise floor rather than the ocean clutter.
- For all linear polarizations considered, the clutter or noise may be characterized as K-distributed. The cross-polarization clutter tended to be more Gaussian than the co-polarization clutter.
- Several ship target RCS metrics were considered. Straightforward model fits provided a relationship between the total RCS and the ship length. The HH and VV total RCS are comparable and similar to previous measurements made with R-1 HH data and with EC CV-580 C-band polarimetric SAR data. The cross-polarization total RCS is about 10 dB smaller than the co-polarization total RCS.
- There is significant variability in the RCS and contrast metrics considered. Focussing on the segmented region RCS-to-clutter ratio, it is apparent that, for co-polarization the contrast increases with increasing incidence angle. This is because the ocean clutter decreases with increasing incidence angle for co-polarization data. On the other hand, for cross-polarization the contrast is more-or-less independent of incidence angle. This is because the noise floor against which the contrast measure is made is essentially independent of incidence angle.
- The ship target contrast is generally larger for larger ships.

- The ship target contrast is best for cross-polarization at smaller incidence angles, and is best for co-polarization at larger incidence angles. The break point between the two cases does depend upon the ship length, but occurs at about 33° incidence angle.
- The total RCS variability was successfully modelled by fitting the normalized total RCS to several well known PDFs. The RCS variability is smaller for cross-polarization ship signatures than for co-polarization ship signatures.
- The estimated ship signature length agreed with the validated ship length for 60.1% of the co-polarization ships and 71.5% of the cross-polarization ships. For co-polarization, the error rate is higher for smaller incidence angles (64.7%) and errors tend to arise from underestimates of the ship length. Similarly, the error rate is higher for smaller TCRs (65.2%). These trends are attributed to higher clutter and lower target contrasts for smaller incidence angles for co-polarization. For cross-polarization, the error rate is also higher for small incidence angles (35.4%), but errors tend to arise from overestimates of ship length. Similarly, the error rate is higher for small TCRs (60.3%), however, there were very few ships that had a contrast smaller than 10 dB in the cross-polarization data. These trends are attributed to the generally higher target contrast providing more visibility for sidelobes or other imaging artefacts at cross-polarization. For all polarizations, there tends to be more overestimates in ship length for azimuth travelling ships.
- Ship wake signatures appear in the cross-polarization channel as a ship-like signature that has not been subject to azimuth shifting, as occurs for the ship signature itself. These signatures appear relatively frequently and may be due to scattering from waves generated off the bow of the ship.

This is a very rich data set that has yielded new observations and insights to ship detectability by SAR. These results could have bearing on the design of future SAR modes or SAR missions, and could be used to improve the performance of ship detection software.

The use of AIS data for ship signature validation is now a well-proven methodology that should be used to develop ship detection models for other missions such as TerraSAR-X and Cosmos-Skymed. Focussing on high density shipping regions would provide a large set of validated ship targets for each image acquired.

References

[1] Vachon, P.W., and Wolfe, J. (2006). Modelling the Probability Density Function of Ship Radar Cross Section Measurements; Analysis of RADARSAT-1 Fine Mode and AISLive Data. DRDC Ottawa TN 2006-271, Defence R&D Canada – Ottawa.

[2] Vachon, P.W., English, R.A., and Wolfe, J. (2007). Validation of RADARSAT-1 Vessel Signatures with AISLive data. *Canadian Journal of Remote Sensing*, Vol. 33, No. 1, pp 20-26.

[3] Vachon, P.W., English, R.A., and Wolfe, J. (2007). Ship Signatures in RADARSAT-1 ScanSAR Narrow B Imagery: Analysis with AISLive Data. DRDC Ottawa TM 2007-052, Defence R&D Canada – Ottawa.

[4] Vachon, P.W., English, R.A., and Wolfe, J. (2007). Ship Signatures in Synthetic Aperture Radar Imagery: Validation using Automatic Identification System Data. Proc. 2007 International Geoscience and Remote Sensing Symposium (IGARSS 2007), 23-27 July 2007, Barcelona, Spain.

[5] European Space Agency, ASAR Public Performance Reports. Available: http://earth.esa.int/pcs/envisat/asar/public_reports/

[6] Blacknell, D. (1994). Comparison of parameter estimators for K-distribution. *IEE Proceedings on Radar, Sonar and Navigation*, Vol. 141, No. 1, pp 45-52.

[7] Vachon, P.W., Dragošević, M., Kashyap, N., Liu, C., Schlingmeier, D., Meek, A., Potter, T., Yue, B., Kraft, J. (2006). Processing and Analysis of Polarimetric Ship Signatures from MARSIE: Report on Results for Polar Epsilon. DRDC Ottawa TM 2006-202. Defence R&D Canada – Ottawa.

[8] Wolfe, J. (2002). VUSAR: A SAR Image Viewer, User Manual. Canada Centre for Remote Sensing, Natural Resources Canada, Ottawa, Ontario.

List of symbols/abbreviations/acronyms/initialisms

A	Ascending
AIS	Automatic Identification System
AO	Announcement of Opportunity
AP	Alternating Polarization
ASAR	Advanced SAR (on Envisat)
CDF	Cumulative Distribution Function
D	Descending
dB	Decibel
DRDC	Defence R&D Canada
EC	Environment Canada
ECDF	Empirical Cumulative Density Function
EOLI	Earthnet OnLine Interactive
ESA	European Space Agency
GUI	Graphical User Interface
HH	Horizontal transmit, Horizontal receive polarization
HV	Horizontal transmit, Vertical receive polarization
EO	Earth Observation
IMO	International Maritime Organization
IS#	Image mode # (ASAR)
ISR	Internet Ships Registry
K-S	Kolmogorov-Smirnov (goodness-of-fit test)
MSVR	Mean-Squared to Variance Ratio
PDF	Probability Density Function
R-1	RADARSAT-1
R&D	Research & Development
RCS	Radar Cross Section
SAR	Synthetic Aperture Radar
SCNB	ScanSAR Narrow B
TCR	Target to Clutter Ratio
VH	Vertical transmit, Horizontal receive polarization
VV	Vertical transmit, Vertical receive polarization

Distribution list

Document No.: DRDC Ottawa TM 2008-005

LIST PART 1: Internal Distribution by Centre:

2 Library
1 Gary Geling
1 Donald Bedard
1 Ryan English
1 Chen Liu
1 Chuck Livingstone
1 Ramin Sabry
1 Jeff Secker
2 Paris Vachon (1 hard copy, 1CD)
1 John Wolfe

12 TOTAL LIST PART 1

LIST PART 2: External Distribution by DRDKIM

1 DRDKIM
3 Library and Archives Canada
1 LCol Jeff Howes, DPDOIS, PM Polar Epsilon
1 LCdr Robert Quinn, DJCP 3-3
1 LCdr Andy Samoluk, DJCP 3-5
1 Caroline Wilcox, DSTC4ISR 5

8 TOTAL LIST PART 2

20 TOTAL COPIES REQUIRED

DOCUMENT CONTROL DATA

(Security classification of title, body of abstract and indexing annotation must be entered when the overall document is classified)

1. ORIGINATOR (The name and address of the organization preparing the document. Organizations for whom the document was prepared, e.g. Centre sponsoring a contractor's report, or tasking agency, are entered in section 8.)

Defence R&D Canada – Ottawa
3701 Carling Avenue
Ottawa, Ontario K1A 0Z4

2. SECURITY CLASSIFICATION (Overall security classification of the document including special warning terms if applicable.)

UNCLASSIFIED

3. TITLE (The complete document title as indicated on the title page. Its classification should be indicated by the appropriate abbreviation (S, C or U) in parentheses after the title.)

Validation of ship signatures in Envisat ASAR AP mode data using AISLive: Data acquisition, processing, and analysis results

4. AUTHORS (last name, followed by initials – ranks, titles, etc. not to be used)

Vachon, Paris W.; Wolfe, John

5. DATE OF PUBLICATION (Month and year of publication of document.)	6a. NO. OF PAGES (Total containing information, including Annexes, Appendices, etc.)	6b. NO. OF REFS (Total cited in document.)
March 2008	66	8

7. DESCRIPTIVE NOTES (The category of the document, e.g. technical report, technical note or memorandum. If appropriate, enter the type of report, e.g. interim, progress, summary, annual or final. Give the inclusive dates when a specific reporting period is covered.)

Technical Memorandum

8. SPONSORING ACTIVITY (The name of the department project office or laboratory sponsoring the research and development – include address.)

Polar Epsilon PMO
and
Defence R&D Canada – Ottawa

9a. PROJECT OR GRANT NO. (If appropriate, the applicable research and development project or grant number under which the document was written. Please specify whether project or grant.)	9b. CONTRACT NO. (If appropriate, the applicable number under which the document was written.)
15ec06-01, 15ec23	

10a. ORIGINATOR'S DOCUMENT NUMBER (The official document number by which the document is identified by the originating activity. This number must be unique to this document.)	10b. OTHER DOCUMENT NO(s). (Any other numbers which may be assigned this document either by the originator or by the sponsor.)
DRDC Ottawa TM 2008-005	

11. DOCUMENT AVAILABILITY (Any limitations on further dissemination of the document, other than those imposed by security classification.)

Unlimited

12. DOCUMENT ANNOUNCEMENT (Any limitation to the bibliographic announcement of this document. This will normally correspond to the Document Availability (11). However, where further distribution (beyond the audience specified in (11) is possible, a wider announcement audience may be selected.))

Unlimited

13. ABSTRACT (A brief and factual summary of the document. It may also appear elsewhere in the body of the document itself. It is highly desirable that the abstract of classified documents be unclassified. Each paragraph of the abstract shall begin with an indication of the security classification of the information in the paragraph (unless the document itself is unclassified) represented as (S), (C), (R), or (U). It is not necessary to include here abstracts in both official languages unless the text is bilingual.)

Ships appear in synthetic aperture radar (SAR) ocean imagery as bright targets against the ocean clutter background. Envisat Advanced SAR (ASAR) Alternating Polarization (AP) mode data acquisitions over the Strait of Dover and the Strait of Gibraltar, two high-density shipping regions with Automatic Identification System (AIS) coverage via AISLive, have provided a large database of validated ship signatures. For each validated ship signature, several metrics were computed including the clutter statistics, the total radar cross section of each ship, and the ship signature length. These metrics were evaluated in terms of the polarization, the local incidence angle, the validated ship length, the target to clutter ratio, and the ship aspect angle. This is a very rich data set that has yielded new observations and insights to ship detectability by SAR. These results could have bearing on the design of future SAR modes or SAR missions, and could be used to improve the performance of ship detection software.

14. KEYWORDS, DESCRIPTORS or IDENTIFIERS (Technically meaningful terms or short phrases that characterize a document and could be helpful in cataloguing the document. They should be selected so that no security classification is required. Identifiers, such as equipment model designation, trade name, military project code name, geographic location may also be included. If possible keywords should be selected from a published thesaurus, e.g. Thesaurus of Engineering and Scientific Terms (TEST) and that thesaurus identified. If it is not possible to select indexing terms which are Unclassified, the classification of each should be indicated as with the title.)

Envisat; Advanced SAR; ASAR; AP mode; alternating polarization mode; SAR; synthetic aperture radar; ship signature; ship detection; AIS; Automatic Identification System

Defence R&D Canada

Canada's leader in Defence
and National Security
Science and Technology

R & D pour la défense Canada

Chef de file au Canada en matière
de science et de technologie pour
la défense et la sécurité nationale

www.drdc-rddc.gc.ca